Springer

KSME

Journal of Mechanical Science and Technology 27 (5) (2013) 1205~1224
www.springerlink.com/content/1738-494x
DOI 10.1007/s12206-013-0401-7

「Review paper」 Mechanical reliability of alloy-based electrode materials for rechargeable Li-ion batteries †

Y. F. Gao[1], M. Cho[2] and M. Zhou[1,2,*]

[1]*The George W. Woodruff School of Mechanical Engineering, School of Materials Science and Engineering, Georgia Institute of Technology, Atlanta, GA30332-0405, USA*
[2]*WCU Program on Multiscale Mechanical Design School of Mechanical and Aerospace Engineering, Seoul National University, Seoul, Korea*

(Manuscript Received January 24, 2013; Revised April 2, 2013; Accepted April 3, 2013)

Abstract

Lithium alloys with metallic or semi-metallic elements are attractive candidate materials for the next-generation high-capacity rechargeable Li-ion battery anodes, due to their large specific and volumetric capacities. The key challenge in the application of these materials has been the very large volume changes, and the associated stress buildup and failure during insertion and extraction of lithium. While such stress buildup bears resemblance to the process of thermo-stress development, a phenomenon relatively well-understood, the physics involved in these alloy-based electrodes is much more complex in nature, more challenging to address, and richer in the variety of influencing factors. The reasons not only lie in the fact that the mechanical deformations are much larger, but also arise from the fact that the processes entail interactions among mass diffusion, chemical reactions, non-linear plastic flow and material property evolutions. In this paper, we present a review of some of the fundamental issues and the latest research related to the mechanical reliability of such alloy-based anode materials, with a focus on Li/Si, a material with the highest known theoretical energy storage capacity. The review primarily concerns continuum-level analyses, with relevant experimental data and atomistic-level results as input.

Keywords: Li-ion battery; Electrode materials; Mechanical reliability; Continuum models; Diffusion; Stress; Plasticity; Fracture

1. Introduction

Energy capacity per unit mass or unit volume is a key figure of merit for battery materials. In the quest for much-needed high energy density and high performance rechargeable batteries for vehicles and portable electronics devices, Li alloys have attracted tremendous interest since it offers greater specific and volumetric capacities than graphite (the negative electrode material for most existing Li-ion batteries) and other candidate materials. One of the main challenges with alloy-based Li-ion battery electrodes, however, has been large volume changes during lithiation and delithiation. For example, when lithiated at room temperature, silicon-based anodes can expand by up to 311% in volume as Li content is changed from 0 to 4.4 per Si [1]. Graphite anodes in commercial batteries, in contrast, exhibit only ~10% volumetric changes [2]. If the alloy-based active material particles are mechanically constrained by a current collector such as the conductive substrate attached to the electrode or the binder which comprises part of the electrode composite, high stresses develop during charge/discharge cycling. Even when mechanical constraints are absent, the inhomogeneity of lithium concentration due to finite lithium diffusivity can still lead to stresses. Such stresses can degrade the electrode material in a few cycles [3], an effect that has hindered the practical application of electrodes based on Li-alloys for almost a decade.

Recent efforts to improve the cyclability of Li-alloy based electrodes are highlighted by the utilization of nano-structured materials [4-7], including Si nanowires (NWs) [8], crystalline-amorphous Si core-shell nanostructures [9], sealed Si nanotubes [10] and nano-structured carbon/silicon composites [11]. Thanks to their ability to reduce diffusion-induced stresses (DIS) and to better accommodate inhomogeneous volume changes, these novel materials can withstand hundreds or thousands of charge/discharge cycles and have enabled the envelop of battery life and allowable charging rates to be pushed out every few months.

The mechanical behavior and failure mechanism of nano-sized electrode materials can be distinctly different from those of electrode material with characteristic sizes in the micron or millimeter ranges. For example, bulk and thin film Si electrodes mainly fail through cracking [1, 12]; Si NW electrodes, on the other hand, may degrade through internal void forma-

*Corresponding author. Tel.: +404 894 3294, Fax.: +404 894 0186
E-mail address: min.zhou@gatech.edu
† Recommended by Associate Editor Moon Ki Kim

tion [13] and/or surface roughening [7]. Sethuraman et al. [14] measured the evolution of stresses in silicon thin films during electrochemical cycling and showed that the flow stress of lithiated Si decreases as Li concentration increases. The finding suggests that parameters which depend on stress singularities such as the mode I fracture toughness K_{IC} are not very relevant for nanostructured Li/Si electrodes. Instead, plastic (or viscoplastic) flow is an important process that cannot be neglected.

Improving the reliability and performance of nano-sized Li-alloy electrode materials requires a fundamental understanding of the complex chemical-mechanical-electrical characteristics of the underlying physical processes and the interplay of many different factors. The multiscale and multiphysics nature of the phenomena involved makes this both a challenging and interesting endeavor which has attracted the attention of many researchers (e.g. Refs. [15-21]). Issues of active studies include concentration-change-induced softening of the alloy materials, inelastic flow, electro-chemical-mechanical coupling, finite deformation and mass transport. This richness of physics presents an opportunity for researchers of solid mechanics to explore novel phenomena which are both theoretically interesting and practically important. The aim of this paper is to present a review of both the underlying issues and the latest research on the mechanical issues related to alloy-based anode materials, especially those based on the Li/Si alloy. The review is mainly focused on the continuum level, with relevant experimental data and atomistic-level results as input.

2. Diffusion-induced stress (DIS)

When lithium is inserted or extracted from an electrode, the volume of the electrode changes. For the Li/Si alloy, such changes can be as large as ~300% [12, 22-24]. Even for LiC_6 electrodes, the lithiation-induced volume changes is non-negligible, although the magnitude of the change is much smaller than that for Li/Si [25]. Such volume changes would almost inevitably lead to stresses. Depending on the design, stresses in an electrode may arise via two mechanisms if the starting material is fully amorphized Si. The first is due to Li concentration inhomogeneity arising from the fact that the diffusivity of Li is finite; the second is due to constraining by external agencies such as a substrate or current collector in contact with the electrode. In section 2.1, we will discuss the first mechanism, namely the development of stress due to Li concentration inhomogeneity. Recent studies concerning the development of stress through the second mechanism will be reviewed in section 2.2. It should be noted that during the first lithiation half-cycle of crystalline silicon (c-Si), amorphization of the material occurs, leading to an amorphous material structure for subsequent cycles [26-28]. Such a phase transition may also induce high levels of stress [29-32]. Many interesting phenomena, including the anisotropic interface mobility and swelling [32-34] and the self-limiting lithiation [35, 36], have been observed during the first half-cycle of c-Si. However, practically feasible Li/Si electrodes would be unlikely to be made from c-Si due to the undesirable effects of the crystalline-amorphous transition [29]. These effects can be avoided by starting with a-Si and/or by allowing electrodes to undergo initial "priming" to bring them to amorphous states. Therefore, discussions in this review mainly focus on situations in which the starting material is fully amorphous. Under this condition, no phase transition and phase boundary between crystalline Si (c-Si) and amorphous Si (a-Si) phases needs to be considered.

The lithiation and delithiation of alloy-based electrodes are electrochemical processes. Still, the electric conductivities of most alloy-based electrodes are high enough so that the electric potential inside the solid domain of the electrode particles can be regarded as uniform. Therefore, most particle-level continuum models of electrode materials entail only the coupling between Li diffusion and mechanical deformation, but not electric fields [15, 17, 37, 38], although exceptions exist [15]. Consideration of electric fields is needed only when the model also considers processes in the electrolyte and the interaction between the electrode and electrolyte. These interactions and the associated microstructural level models are to be reviewed in section 6.

2.1 Diffusion-induced stresses in free-standing particles

The analyses of free-standing particles allow stress development due to concentration inhomogeneity and diffusion to be quantified. When an electrode made of free-standing particles is subject to charge or discharge, Li concentration in each particle is inhomogeneous because of the finite diffusivity of Li. Consequently stresses build up. The buildup of stresses due to composition inhomogeneity during diffusive transport in solid materials is a ubiquitous process seen in many disciplines of science and engineering. Such stresses, called "diffusion-induced stresses" (DIS), has been observed in many areas including oxidation of metals, hydrogen transport in solid-state hydrogen-storage media, dopant diffusion in semiconductor processing, and lithium ion transport in battery electrodes. One of the earliest analyses of DIS was conducted by Prussin who drew analogy between thermal stress and DIS [39]. Since then, numerous studies have been devoted to analyzing the DIS problems in various geometric configurations [40-43]. Later, Yang extended the Prussin model by considering the coupled interaction between stress and diffusion [44].

Due to its close relationship with cyclic degradation, DIS in free-standing particle electrodes has been subject to extensive studies. By drawing an analogy to the thermal stress problem, Cheng and collaborators analyzed the effect of DIS in battery electrode particles with spherical [45, 46] and cylindrical [47] shapes. They discussed the implications of different charging regimens such as potentialstatic and galvanostatic operations on stress levels [45]. They also identified a dimensionless number that is analogous to the Biot number in heat transfer problems in order to quantify the relative significance of sur-

face kinetics, governed by linearized Butler-Volmer's law [cf. Eq. (17)], and the bulk diffusion kinetics, governed by the Fick's law [48]. The effect of surface tension on internal stress in spherical particles has been investigated, and it is suggested that the surface effect can significantly reduce the tensile stress in the material when the particle radius is shrank into the nano regime [19].

Christensen and Newman [25] developed a mathematical model that allows calculation of the volume changes and the profiles of concentration and stress during lithium insertion and extraction from a spherical particle. In developing the model [25], they not only considered non-ideal interactions between lithium and host material, but also incorporated the effect of pressure-driven diffusion, making the model one of the earliest that consider two-way deformation-diffusion coupling in battery electrodes. The implication of such two-way coupling between deformation and diffusion will be discussed in section 4. In terms of DIS, it is found that the maximum stress in a spherical carbonaceous particle is controlled by a dimensionless current

$$I = \pm \frac{CR_0^2 x_{\max}}{3D_{LiS,S}} \tag{1}$$

where C is the so-called C-rate, namely the inverse of the time required for full lithiation or delithiation, R_0 is the initial particle radius, and $D_{LiS,S}$ is the diffusivity of the Li-host compound (LiS) relative to the host material (referred to as the binary diffusion coefficient by Christensen and Newman). A positive I indicates lithiation while a negative I stands for delithiation. Fig. 1 shows the maximum compressive and tensile stresses, normalized by the Young's modulus, encountered during galvanostatic lithium insertion into a spherical carbonaceous particle. The maximum tensile stress [**a** and **c**], which occurs at the center of the particle, and the maximum compressive stress [**b** and **d**], which occurs at the surface, are plotted against the dimensionless current given by Eq. (1). In order to study the effect of non-ideality of the binary LiC solution, a thermodynamic factor α_{LiC} is introduced [25]. When $\alpha_{LiC} = 1$ the model reduces to the ideal solution case. For the more realistic, non-ideal solution cases, α_{LiC} can be derived from experimentally-measured open-circuit potential (OCP) curves. As seen in Fig. 1, the stress maxima for ideal solution cases (**c** and **d**) scale almost linearly with the dimensionless current I. For the non-ideal solution cases (**a** and **b**), the relationship between the stresses and the dimensionless current deviates from linearity, but the general trend that stresses increase with I remains. The results in Fig. 1, together with Eq. (1), therefore indicate that stresses, hence the fracture tendency, are higher when the C-rate is higher and when the particle radius R_0 is larger. It can also be concluded that a higher diffusivity $D_{LiS,S}$ helps reduce stress and hence decrease the likelihood of fracture. A similar scaling law between stress and dimensionless current I has also been found for the $LiMn_2O_4$ cathode material [49, 50].

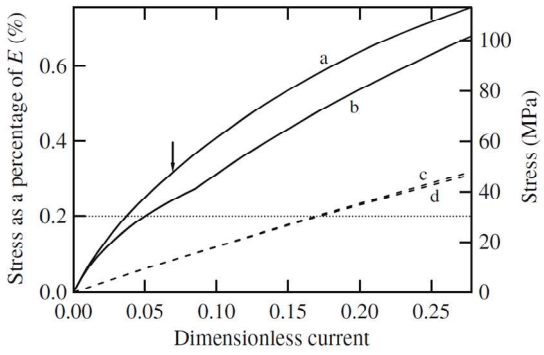

Fig. 1. The maximum tensile: (a) and compressive; (b) stresses calculated using a realistic thermodynamic factor for LiC_6, and the maximum tensile; (c) and compressive; (d) stresses calculated using an ideal thermodynamic factor of unity, as functions of dimensionless current. The arrow marks the dimensionless current corresponding to a 5-μm particle radius and 5C charge rate. Reproduced from Ref. [25] with permission.

The scaling law embodied in Eq. (1) and Fig. 1 has turned out to be the primary impetus for the recent research of nano-sized electrode materials [5-7, 10, 11, 21, 51]. Although the definition of the dimensionless current in Eq. (1) is for spherical-shaped particles, the conclusion that stresses scale with the square of size (R_0^2) can be quite universal, as long as R_0 is construed as the characteristic length of the material. For cylindrical-shaped particles, for example, R_0 can be identified to be the radius of the cylinder, and the stresses again scale with R_0^2 during lithiation and delithiation.

If carbon is replaced by alloy-based materials, such a scaling law gains even more importance since failure due to DIS is a much more pronounced issue [8]. By reducing the particle size to the nano-scale, one significantly reduces the stresses and hence fracture tendency. One of the earliest attempts in using silicon nanowires (NWs) as an anode material is made by Chan et al. [8], who achieved the theoretical charge capacity for silicon anodes and maintained a discharge capacity close to 75% of the theoretical maximum, with little fading during cycling. Besides the reduction of stresses, another benefit of using NWs, according to Chan et al. [8], is the maintenance of good electronic contact with the substrate as illustrated in Fig. 2.

2.2 Diffusion-induced stresses in thin-film electrodes

The stress build-up mechanism due to composition inhomogeneity reviewed in section 2.1 is relevant for electrode materials made of free-standing particles. If the electrode material is constrained by external agencies such as a substrate or current collector, stresses can arise even when the Li concentration is homogeneous. This is the case for thin-film electrodes, in which the active electrode material (e.g., Si or Sn) is deposited on a current collector, usually made of Cu or Ti, via thin-film deposition techniques such as electron beam evaporation or sputtering [14, 52, 53]. The constraints due to the

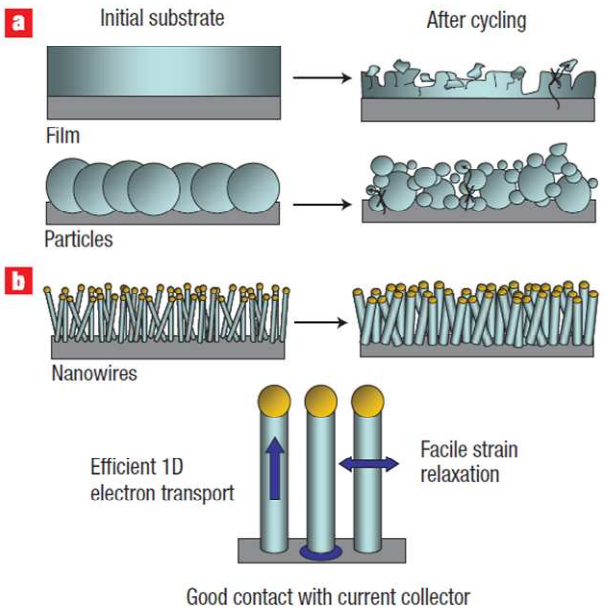

Fig. 2. Schematic illustration of morphological changes that occur in Si during electrochemical cycling: (a) The volume of silicon anodes changes by about 300% during cycling. As a result, Si films and particles tend to pulverize during cycling. Much of the material loses contact with the current collector, resulting in poor transport of electrons, as indicated by the arrow; (b) NWs grown directly on the current collector do not pulverize or break into smaller particles after cycling. Rather, facile strain relaxation in the NWs allows them to increase in diameter and length without breaking. This NW anode design has each NW connecting with the current collector, allowing for efficient 1D electron transport down the length of every NW. Reproduced from Ref. [8] with permission.

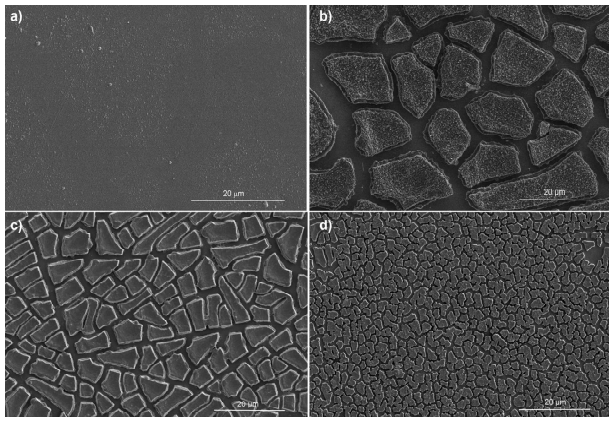

Fig. 3. Crack patterns in thin-film Li/Si electrodes that form due to electrochemical cycling: (a) An SEM image of a 500 nm a-Si film before electrochemical tests and (b-d) crack patterns on a-Si thin films of different thicknesses; (b) 1000 nm thick, after 5 cycles; (c) 500 nm thick, after 5 cycles; (d) 200 nm thick, after 10 cycles. Reproduced from Ref. [54] with permission.

bonding between the film and the current collector typically lead to high stresses and fracture patterns as shown in Fig. 3 [54]. Similar crack patterns are also seen in other Li-alloy-based electrode material systems, such as Ge [55], Sn [56], and Si-Sn [12]. To analyze such fracture patterns, Li et al. [54] modified the two-dimensional spring-block model originally proposed by Leung and Neda [57] for the problem of corn starch drying, and successfully explained the experimental observation that cracks are straight with larger islands in thicker films, but show more wiggles with smaller islands in thinner films [cf. the SEM images in Fig. 3]. The analysis by Li et al. [54] also shows a critical film thickness below which no crack would form in Li/Si thin-film electrodes. Indeed, for Li/Si films with thicknesses below 100 nm, experiments [54] show that interconnected cracks do not form up to 10 cycles of lithiation/delithiation. The estimation of such a critical thickness h_c is based on the Griffith's fracture criterion, according to which h_c is given by [54, 58]

$$h_c \approx 4\sqrt{2}\frac{G_c E}{\sigma^2\left(1-\nu^2\right)} \tag{2}$$

where E and ν are Young's modulus and Poisson's ration, respectively; σ is the stress in the thin film; and $G_c = K_{Ic}^2 / E$ is the plane-stress fracture toughness of the active electrode material in terms of critical energy release rate. Taking $K_{Ic} = 1$ MPa m$^{1/2}$ (which leads to $G_c \sim 10$ J/m^2, a fairly high estimation) and $\sigma = 2$ GPa, Li et al. [54] estimated that h_c for Li/Si is on the order of several hundred nanometers, most likely between 100 nm and 200 nm.

The expression in Eq. (2) clearly captures the fact that reducing the film thickness suppresses fracture. It turns out that reducing the in-plane dimensions of the islands of active materials also mitigates fracture in Li/Si thin-film electrodes [53]. As mentioned before, the stresses in thin-film electrodes arise mainly due to the constraints at the film-substrate interface. Weaker constraints, for example in the form of interfacial sliding, may therefore be beneficial because it helps reduce the stress level. Xiao et al. [53] leveraged this idea by introducing a patterning approach to improve the cycling stability of silicon electrodes (Fig. 4(a)). They found an improvement in cycle life when the pattern size is below the critical (7-10 μm) level. To explain the mechanism responsible for their observation, Xiao et al. [53] considered a Si thin film which already contains an array of cracks with spacing L and raised the question whether there exists a minimum crack spacing which is small enough so that no additional crack can be inserted between the existing cracks. They assumed that the additional crack would form via plastic strain localization between two neighboring cracks in Si. Considering the free body diagram shown in Fig. 4(c), they found that the critical spacing below which no new crack can be inserted is

$$L_{cr} = \frac{2\sigma_Y^{Si}}{\tau_{cr}^{\text{int}}} h \tag{3}$$

where h is the film thickness, σ_Y^{Si} is the yield stress of Si,

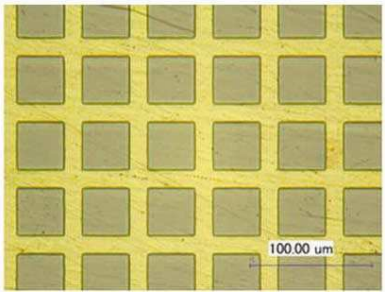

(a)

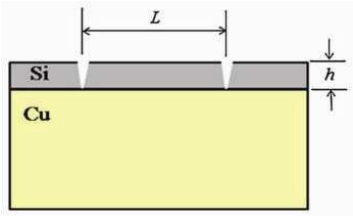

(b)

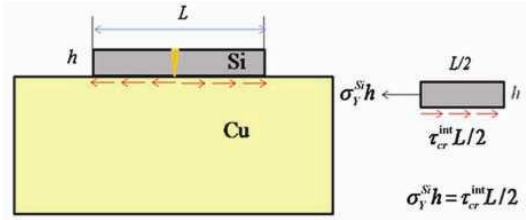

(c)

Fig. 4. The design and fracture process of patterned Li/Si thin-film electrodes: (a) SEM image of Si pattern on Cu substrate with pattern width around 40 μm. The experiments conducted by Xiao et al. [53] were carried out for pattern widths from 7 μm to 40 μm; (b) The configuration of a Si film with a periodic array of cracks of spacing L on Cu substrate; (c) The minimum crack spacing that could no longer allow an extra crack to be formed in between the existing cracks. Below this minimum crack spacing, the stress in the lithiated Si film could not reach its plastic yield stress and therefore no strain localization in the film can take place to form an additional crack. Reproduced from Ref. [53] with permission.

and τ_{cr}^{int} is the interfacial shear strength between lithiated Si and Cu substrate. It is estimated from Eq. (3) that the critical spacing is $L_{cr} \sim 5.1-8.9\,\mu\text{m}$, in agreement with experiments. The assumptions behind this model, especially the assumption that a film with smaller pattern spacing has lower stresses ($\sigma < \sigma_Y^{Si}$) due to interfacial sliding and therefore deforms elastically, were later confirmed to be valid by in situ measurements of stress [59, 60].

Note that Eq. (3) concerns the plastic deformation and hence failure of the Si film itself, but not the delamination at the Si/Cu interface which is also observed in experiments. To address the latter issue, a more sophisticated model was developed by Haftbaradaran et al. [61]. This model is an extension of the physical picture depicted in Fig. 4 and leads to yet another length scale that controls the peal-off of the cracked Si film from the Cu substrate.

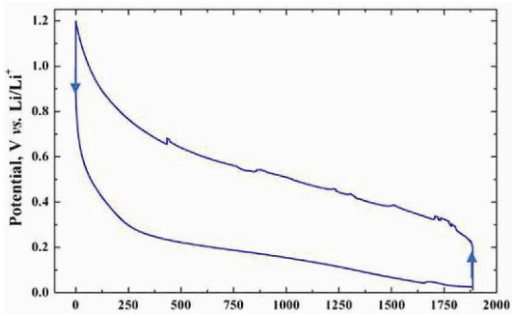

(a)

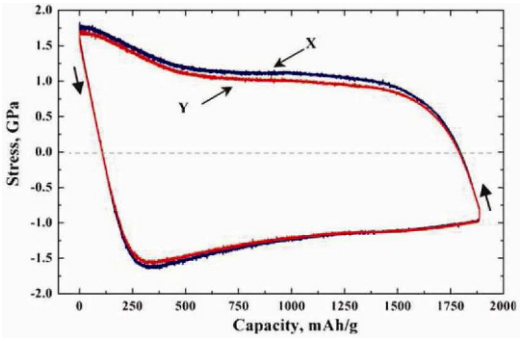

(b)

Fig. 5. (a) Cell potential vs capacity curve corresponding to lithiation and delithiation of a-Si thin-film electrode cycled at C/4 rate between 1.2 and 0.01 V vs. Li/Li$^+$; (b) the corresponding stress calculated from the substrate curvature using the Stoney equation. The curves labeled X and Y correspond to the stresses calculated from the averaged horizontal and vertical displacements of the spots, respectively. The arrows in both figures indicate cycling direction. Reproduced from Ref. [14] with permission.

3. Plastic deformation and lithiation-induced softening of Li/Si

Although pure silicon in its crystalline or amorphous state is brittle [62], lithiated Si, which is generally amorphous, can undergo significant inelastic deformation. Such a brittle-to-ductile transition of Li/Si is an important embodiment of an effect called "lithiation-induced softening". There are two aspects of lithiation-induced softening of Li/Si: reduction in yield stress and reduction in elastic modulus as the Li content increases. This section reviews the experimental data available, the underlying mechanisms as revealed by atomistic calculations, and the continuum models used to deal with the large inelastic deformations when electrode materials become ductile.

3.1 Experimental observations and atomistic mechanisms

Sethuraman et al. employed an experimental technique with a multi-beam optical sensor (MOS) to measure the in-situ stress evolution in a thin-film Si electrode [63]. The technique entails the measurement of the curvature change of the film-substrate system during electrochemical cycling and the calculation of the stresses in the thin film from the curvature via the Stoney equation [60, 64]. Fig. 5 shows the cell potential and

the film stress so obtained as functions of the capacity of the silicon thin-film electrode [14]. This capacity level (the horizontal axis) is linearly related to the Li content ξ in the chemical composition $Li_\xi Si$. During the lithiation process, an initial linear increase in the bi-axial compressive stress is attributed to elastic deformation. At compressive stress of about 1.7 GPa (which corresponds to a capacity of *ca.* 325 $mAhg^{-1}$), the film appears to reach the elastic limit and begins deform inelastically with further lithiation. This response is needed in order to accommodate the additional volume expansion. The flow stress is seen to decrease with further lithiation, reaching a value of about 1 GPa at a capacity of *ca*. 1875 $mAhg^{-1}$, at the cut-off potential. Upon delithiation, the unloading is initially elastic; the stress reverses elastically until it reaches *ca*. 1 GPa in tension, where the film begins to flow in tension in order to accommodate the reduction in volume. The flow stress increases to about 1.75 GPa when the upper limit of 1.2 V is reached. What Sethuraman et al. [14] observed clearly indicates that lithiated Si undergoes inelastic deformation, and the associated yield stress σ_Y decreases as the Li content ξ in $Li_\xi Si$ increases. Such a decrease in σ_Y is an important manifestation of what is called lithiation-induced softening.

In terms of the atomistic mechanisms that underlie the observed behavior, Zhao et al. [65] proposed that the brittle-to-ductile transition with increasing Li concentration and associated large plastic deformation is due to continuous lithium-assisted breaking and re-forming of Si-Si bonds and the creation of nanopores.

Besides the decrease in σ_Y, the effect on mechanical properties of Li/Si of lithiation also entails the decrease in elastic moduli [63, 66, 67]. One of the earliest studies on the elastic softening of Li-Si due to lithiation was by Shenoy et al. [67], who carried out density functional theory (DFT) calculations of the elastic moduli of a-Si and c-Si in different lithiation states. As shown in Fig. 6, they found that the elastic properties of a-Si and c-Si depend strongly on the lithiation state, i.e. the ξ value in the chemical formula $Li_\xi Si$. This dependence approximately follows the rule of mixing that connects the elastic properties of $Li_\xi Si$ at the two end compositions, i.e. $\xi = 0$ and $\xi = \xi_{max}$. In terms of atomistic mechanism, they attributed the elastic softening to the increase in the population of ionic Li–Si bonds that are weaker than the covalent Si–Si bonds [67].

Hertzberg et al. [66] arrived at a conclusion consistent with those drawn by Sethuraman et al. [14] and Shenoy et al. [67] for the Young's modulus and hardness through ex-situ depth-sensing indentation experiments. The measurements by Hertzberg et al. [66] indicate that the Young's modulus decreases from an initial value of 92 GPa for pure Si to 12 GPa at full lithium insertion (Li_5Si_4), and the corresponding hardness change is from an initial value of 5 GPa for Si to 1.5 GPa for $Li_{15}Si_4$. The measured modulus-concentration dependence by Hertzberg et al. deviates slightly from the simple rule of mixing suggested by the DFT calculations of Shenoy et al. [67]. Such a deviation could have important implications, but

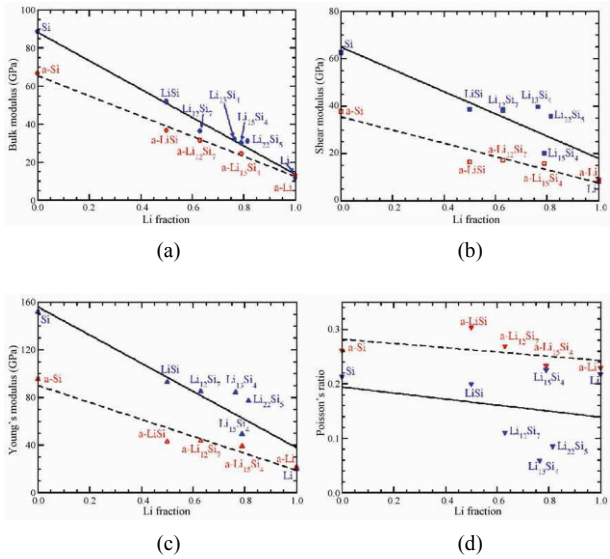

Fig. 6. (a) Bulk modulus *B*; (b) shear modulus *G*; (c) Young's modulus *E*, and (d) Poisson's ratio ν of Li–Si alloys plotted as functions of Li fraction in crystalline (solid symbols) and amorphous (open symbols) phases for the alloy $Li_\xi Si$. The Li fraction in the alloy is given by $\xi/(1+\xi)$. Solid and broken lines show linear fits for the crystalline and the amorphous systems, respectively. Reproduced from Ref. [67] with permission.

is nevertheless considered to be as higher-order effect in most continuum models that consider the lithiation-induced softening (e.g. Refs. [15, 37, 68]). These studies adopt the rule of mixing for simplicity.

In continuum theories, the lithiation-induced changes in mechanical properties are usually modeled by assuming that the elastic moduli and yield stress are functions of the local lithium concentration [15, 37, 69], an assumption that is sufficient for capturing most experimental observations with regard to the effects of lithiation-induced softening. More sophisticated theories have also been proposed. For example, it is suggested by Brassart and Suo that the link between mechanical response and electrochemical charging conditions can also be established by reckoning the non-equilibrium driving force $\Omega^{Li}\varsigma$ which is essentially the difference in chemical potentials between the electrode material and the surrounding environment [70, 71]. Here, Ω^{Li} is the partial atomic volume of Li and ς is the osmosis pressure. The key assumption behind this type of treatment is that the concurrent deformation and reaction processes is a non-equilibrium process which is governed by how far the state deviates from thermodynamic equilibrium. Many interesting predictions have been made out from this type treatment, including the prediction that the host under a constant deviatoric stress will flow gradually in response to ramping in the chemical potential, and will ratchet in response to cycling in the chemical potential [70].

3.2 Kinematics of large inelastic deformation

The fact that Li/Si undergoes elastic-plastic or elastic-

viscoplastic deformations indicates that the continuum constitutive laws governing the mechanical response must be cast in an incremental or time-rate form. Such continuum-level descriptions usually entail the decomposition of the total deformation into three parts: a plastic part which corresponds to the irrecoverable volume-conserving shape change, an expansion part which corresponds to the volume change due to lithiation/delithiation, and an elastic part which is usually small and recoverable. Mathematically, the decomposition can be carried out by decomposing the total strain [19, 50, 72], the total stretch [38], or the total deformation gradient [15, 17, 20, 37, 73]. The third approach, decomposition of the total deformation gradient $\mathbf{F}$, admits the convenient treatment of finite deformations and rotations – processes that are indeed observed in Li/Si and other alloy-based electrode materials. This decomposition is therefore most often used. In this approach, which is originally proposed by Lee [74], $\mathbf{F}$ is multiplicatively decomposed as

$$\mathbf{F} = \mathbf{F}^e \cdot \mathbf{F}^{SF} \cdot \mathbf{F}^p \tag{4}$$

where $\mathbf{F}^e$, $\mathbf{F}^{SF}$ and $\mathbf{F}^p$ are the elastic, stress-free volumetric and plastic deformation gradients, respectively. Here, the plastic part $\mathbf{F}^p$ is volume-conserving [i.e., $\det\left(\mathbf{F}^p\right)=1$], and the volumetric part $\mathbf{F}^{SF}$ is termed "stress-free" because it corresponds to the shape changes of the material due to composition change without stress. One assumption that is typically made for amorphous silicon (a-Si) is that $\mathbf{F}^{SF}$ is isotropic, although the theoretical framework depicted by Eq. (4) by itself does not require such isotropy and can also be used for situations where $\mathbf{F}^{SF}$ is anisotropic.

The decomposition in Eq. (4) implies linking the reference (or Lagrangian) state and the current (or Eulerian) state via two imaginary and incompatible states, as shown in Fig. 7. When a piece of electrode material is lithiated from the top layer, the top part expands in the actual charged state, leading to deformation gradient $\mathbf{F}$ and associated stresses. This total deformation gradient is decomposed such that the material first deforms plastically to reach incompatible state I, and then undergoes expansion $\mathbf{F}^{SF}$ to reach incompatible state II. Here incompatible states I and II are stress-free but discontinuous. To maintain continuity, an elastic accommodation $\mathbf{F}^e$ is needed. This elastic deformation pieces the incompatible state II together back to the actual charged and stressed state.

Given the Lee decomposition delineated in Eq. (4) and Fig. 7, the mechanical properties of an electrode material can be prescribed by laying out the constitutive equations that govern $\mathbf{F}^e$, $\mathbf{F}^{SF}$ and $\mathbf{F}^p$ one by one. Usually, $\mathbf{F}^{SF}$ is assumed to be isotropic for amorphous alloy electrode materials, such as a-Si. Further, it is assumed to depend only on the composition (ξ value in chemical formula $\mathrm{Li}_\xi\mathrm{Si}$). A linear relationship between $J^{SF}(\xi)=\det\left(\mathbf{F}^{SF}\right)$ and ξ is used by most continuum models [15, 37]. The isotropic Hook's law is typically used for $\mathbf{F}^e$, which nevertheless should be cast into an objective

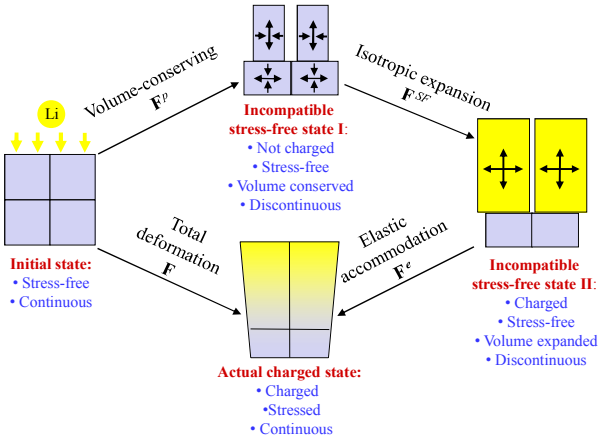

Fig. 7. Illustration of the Lee-type decomposition. The total deformation gradient $\mathbf{F}$ is decomposed into three parts linked by two incompatible stress-free states.

rate form in order to allow for large deformations [15, 20]. For $\mathbf{F}^p$, most researchers use J_2-type associated flow rules which can be either plastic [38, 75, 76] or viscoplastic [15, 37]. Different types of governing equations for the elastic, stress-free volumetric and plastic deformation components are summarized in Table 1.

The decomposition of the total deformation and the associated constitutive laws for each decomposed part described in Table 1 govern what is called the "chemical-to-mechanical coupling", i.e., how chemical diffusion gives rise to mechanical deformation and stresses. Indeed, most models reviewed in section II are more or less based on this approach, despite many of them [19, 45-48, 50, 77-80] are based on decomposition of strains instead of the deformation gradient and hence are small-deformation theories. This chemical-to-mechanical coupling, however, is but one aspect of the chemo-mechanical two-way coupling. While diffusion induces stresses, stresses can also affect diffusion. The physical picture, mathematical model and practical implications of such two-way coupling will be discussed in the next section.

4. Chemical-mechanical two-way coupling

The chemo-mechanical two-way coupling involves two aspects, chemical-to-mechanical (CM) coupling and mechanical-to-chemical (MC) coupling. The theoretical framework for CM coupling is based on the decomposition of deformation described in section 3.2. This section mainly concerns the mechanical-to-chemical coupling, i.e., the effect of stresses on diffusion. There are mainly two approaches for MC coupling in alloy-based electrode materials. The first is via a dependence of chemical potential on stress, and the second is via a dependence of the activation energy barrier on stress.

4.1 Stress-induced chemical potential shift

The physical picture of mechanical-to-chemical coupling

Table 1. Governing equations for the elastic, stress-free expansion, and plastic components of total deformation.

Component	Governing equation		Relevant variables	Ref.
Elastic ($\mathbf{F}^e$)	Total form: $\sigma_{ij} = F^e_{iK}\left(3K\varepsilon^e_m\delta_{KL} + 2G\varepsilon^{e'}_{KL}\right)F^e_{jL}$ Rate form: $\mathbf{D}^e = \left(\frac{1}{9K} - \frac{1}{6G}\right)tr\left(\overset{\circ}{\boldsymbol{\sigma}}\right)\mathbf{I} + \frac{\overset{\circ}{\boldsymbol{\sigma}}}{2G}$		σ_{ij} : Cauchy stress $\varepsilon^{e'}_{KL}$, ε^e_m : Deviatoric and hydrostatic parts of elastic strain K, G : Concentration-dependent bulk and shear moduli $\mathbf{D}^e$: Elastic rate of deformation $\overset{\circ}{\boldsymbol{\sigma}}$: Objective rate of $\boldsymbol{\sigma}$	[15, 17, 47]
Stress-free expansion ($\mathbf{F}^{SF}$)	$J^{SF} = 1 + \eta\xi$		$J^{SF} \equiv \det\left(\mathbf{F}^{SF}\right)$: Volume ratio associated with $\mathbf{F}^{SF}$ ξ : ξ in $\mathrm{Li}_\xi\mathrm{Si}$ η : Volume expansion rate	[15, 19, 37, 38, 68]
Plastic ($\mathbf{F}^P$)	Plastic	$\left.\begin{array}{l}\mathbf{D}^P = \dot{\lambda}\frac{\partial Q}{\partial\boldsymbol{\sigma}}, \text{ when } Q \ge 0,\\ \mathbf{D}^P = 0, \quad \text{when } Q < 0.\end{array}\right\}$, with Type I (ref. [69, 75]): $Q = \frac{1}{2}\boldsymbol{\sigma}^{dev}:\boldsymbol{\sigma}^{dev} - \frac{1}{3}\left(\sigma_Y\right)^2$, with $\sigma_Y = \sigma_Y\left(\xi\right)$. Type II (ref. [70, 71]): $Q = \frac{1}{2}\boldsymbol{\sigma}^{dev}:\boldsymbol{\sigma}^{dev} + q\varsigma^2 - \frac{1}{3}\left(\sigma_Y\right)^2 = 0.$	Q : Flow potential. $\mathbf{D}^P$: Plastic deformation rate. $\boldsymbol{\sigma}^{dev}$: Deviatoric component of $\boldsymbol{\sigma}$. σ_{mises} : Von Mises invariant of Cauchy stress. σ_Y : Yield threshold. ς : Osmotic pressure q : Constant controlling reactive flow.	[69-71, 75]
	Visco-plastic	$\mathbf{D}^P = \frac{\partial Q}{\partial\boldsymbol{\sigma}^{dev}}$, with $Q = \frac{\sigma_Y\dot{d}_0}{m+1}\left(\frac{\sigma_{mises}}{\sigma_Y} - 1\right)^{m+1} H\left(\frac{\sigma_{mises}}{\sigma_Y} - 1\right)$	H : Heaviside step function. $\dot{d}_0$: Reciprocal of viscosity. m : Stress exponent.	[15, 37]

via stress-induced chemical potential shift is rather simple. Consider a piece of $\mathrm{Li}_\xi\mathrm{Si}$ alloy in which ξ is spatially homogeneous. If one side of the alloy is compressed and the other side is stretched, the resultant stress gradient would induce a driving force that squeezes lithium from the compressive side to the tensile side, as shown in Fig. 8.

One of the earliest models that considers such an effect was developed by Christensen and Newman [25] who identified three different types of stress: total stress, elastic stress, and the thermodynamic pressure. The mechanical-to-chemical coupling takes effect via the thermodynamic pressure. The Newman model, in essence, is a model that invokes a decomposition that is similar to that in Fig. 7, although the decomposition is not for deformation but for stress. It can be proved that the two approaches, or the decompositions of deformation (i.e., strains or deformation gradient) and stress, are equivalent, at least when the material deforms elastically [25]. However, when plastic deformation needs to be considered, the Newman approach is inconvenient and later models [15, 37] mostly have adopted the decomposition in Fig. 7. The result is a mechanical driving force to diffusion that manifests itself as a stress-induced chemical potential change.

The key here is that the MC coupling takes place via the chemical potential μ^{Li}, such that [17, 81]

$$\mu^{Li} = \left.\frac{\partial\phi}{\partial C^{Li}}\right|_{\mathbf{F}^e,\theta} - \det\left(\mathbf{F}^e\right)\Omega^{Li(SF)}\sigma_m \tag{5}$$

where $\sigma_m \equiv \sigma_{kk}/3$ is the hydrostatic stress, C^{Li} is the Lagrangian density of lithium, $\Omega^{Li(SF)} \equiv \partial J^{SF}/\partial C^{Li}$ is the stress-free partial atomic volume of lithium, $J^{SF} = \det\left(\mathbf{F}^{SF}\right)$ is the ratio of volume change (or the Jacobian of the deformation gradient) due to composition change, θ is temperature, and $\phi = \phi(\mathbf{F}^e, C^{Li}, \theta)$ is the Lagrangian density of the Helmholtz free energy. For most relevant cases, the elastic strain associated with $\mathbf{F}^e$ is small. Under such conditions, the expression for the chemical potential (Eq. (5)) can be simplified into

$$\mu^{Li} = \mu^{Li}_{SF} - \det\left(\mathbf{F}^e\right)\Omega^{Li(SF)}\sigma_m \approx \mu^{Li}_{SF} - \Omega^{Li(SF)}\sigma_m \tag{6}$$

with

$$\mu^{Li}_{SF} = \partial\phi^{SF}/\partial C^{Li} = \mu^{Li}_{SF}\left(C^{Li}\right) \tag{7}$$

being the chemical potential of lithium at zero stress. Generally speaking, $\mu^{Li}_{SF}\left(C^{Li}\right)$ can be determined by fitting the activity coefficient to experimentally measured open circuit potential (OCP) data [25, 68, 82]. It can also be mathematically given if one makes simplifying assumptions such as the

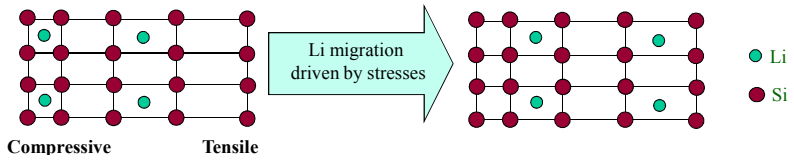

Fig. 8. Illustration of lithium migration driven by mechanical stress. Such an effect can be described by considering a stress-induced chemical potential shift.

ideal solution assumption [19, 38, 77, 83, 84], regular solution assumption [85-87], or lattice-gas assumption [88-90], depending on the need and level of sophistication of the model.

The second term in Eq. (6) is a stress-induced shift of the chemical potential. When μ^{Li} is substituted into the Fick's law [73] in the form of

$$J_K^{Li} = -\frac{D^{Li}}{k_B\theta} f_{Ki} f_{Ji} C^{Li} \frac{\partial \mu^{Li}}{\partial X_J} \tag{8}$$

the effect of Li migration driven by stress gradients (cf. Fig. 8) is captured. Note that the stress-induced chemical potential shift is positive in compressive regions and negative in tensile regions, and the associated diffusive flux is towards the negative of the chemical potential gradient. In Eq. (8), J_K^{Li} is the chemical flux measured in the reference configuration, $\mathbf{f} = \mathbf{F}^{-1}$ is the inverse of the deformation gradient, D^{Li} is the diffusivity of Li., k_B is the Boltzmann constant, and $\partial / \partial X_J$ stands for spatial gradient in the reference configuration.

Questions arise when it comes to the relative importance of the stress-free part μ_{SF}^{Li} and the stress-induced shift $-\Omega^{Li(SF)}\sigma_m$ in terms of their contributions to the Li flux. It will be shown in section 4.3 that, to incorporate $-\Omega^{Li(SF)}\sigma_m$ into the diffusion model, the stress gradient $\nabla_{\mathbf{X}}\sigma_m$ is needed, and considerable effort [17, 91] is required to numerically capture $\nabla_{\mathbf{X}}\sigma_m$ in a finite element (FE) framework. If the contribution to flux due to $-\Omega^{Li(SF)}\sigma_m$ is much smaller than that due to μ_{SF}^{Li}, it might be economical and prudent to neglect the stress-induced chemical potential shift and, hence, the mechanical-to-chemical coupling at together. However, Gao and Zhou [68] showed that the contribution of mechanical-to-chemical coupling (MC) to diffusion driving forces is very significant compared with the contribution of purely chemical driving forces and, therefore, cannot be neglected. To show this they considered a silicon NW lithiated under galvanostatic conditions. The lithiation speed is slow enough such that stresses in the NW are below the yield threshold and elastic response is maintained. Under this elastic condition, the effect of MC coupling can be lumped into an effective diffusivity D_{eff}^{Li} [21, 50, 68, 73], such that Eq. (8) can be simplified into

$$\begin{cases} J_K^{Li} = -D^{Li,eff} f_{Ki} f_{Ji} \dfrac{\partial C^{Li}}{\partial X_J}, \text{ where} \\ D_{eff}^{Li} = D^{Li} \dfrac{\Phi^{Li}}{1+\xi} + \dfrac{D^{Li}}{k_B\theta} \dfrac{2E\left(\Omega^{Li(SF)}\right)^2}{9(1-\nu)} \dfrac{C^{Li}}{\det\left(\mathbf{F}^{SF}\right)}. \end{cases} \tag{9}$$

Here, Φ^{Li} is the stress-free thermodynamic factor for diffusion [25], which is usually greater than 1 and can be estimated from open-circuit potential data. ξ is the Li content in the chemical formula $Li_\xi Si$, and ν is the Poisson's ratio. Using Eq. (9), Gao and Zhou [68] obtained analytical solutions for concentration and stresses, and found significant contributions to the driving force for diffusion due to mechanical-to-chemical coupling. Such contributions lead to an increase of 303% in the effective diffusivity of lithium compared with situations without the MC coupling effect. The effect is therefore termed the stress-enhanced diffusion (SED). This SED effect makes the long-term profiles of the dimensionless concentration ξ more uniform [cf. Fig. 9(c)]. Similar effects of the SED are also found in cathode materials such as $LiMn_2O_4$ and the anode lattice of LiC_6 [25, 50, 92], as seen in Figs. 9(a) and 9(b). However, the SED in Li/Si is much stronger than those in $LiMn_2O_4$ and LiC_6, in the sense that the change in concentration profiles due to SED (i.e. the difference between the solid and dashed lines) is much larger for Li/Si than those seen for the other two materials.

The fact that the mechanical-to-chemical coupling, or the effect of SED, is much more pronounced in Li/Si than that in other intercalation materials is attributed to two reasons [68]. First, the partial atomic volume $\Omega^{Li(SF)}$ in Li/Si is much larger than those in $LiMn_2O_4$ and LiC_6 -- according to Eq. (9) the MC contribution to the effective diffusivity (second term) is proportional to the square of $\Omega^{Li(SF)}$. Second, Li/Si can be charged to a much higher Li concentration limit than cathode lattices or carbon -- and the MC contribution to D_{eff}^{Li} is proportional to the concentration. Therefore, the mechanical-to-chemical coupling in Li/Si has significant implications and cannot be neglected.

4.2 Activation barrier shift

Besides shifting the chemical potential, mechanical stress may also affect diffusion by shifting the activation barrier [18, 93], such that the diffusivity is modulated by stress according to

$$D^{Li} = D_0^{Li} \exp\left(\frac{\alpha \Omega^{Li(SF)} \sigma_b}{k_B\theta}\right) \tag{10}$$

where α is a positive dimensionless constant, $\Omega^{Li(SF)}$ is the partial atomic volume of Li, D_0^{Li} is the diffusivity under zero stress, and σ_b is the biaxial stress perpendicular to the di-

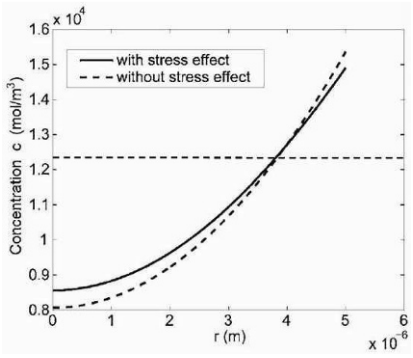

(a)

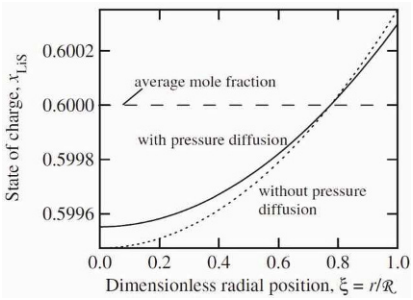

(b)

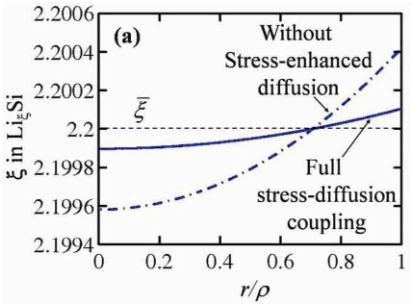

(c)

Fig. 9. Typical concentration profiles during galvanostatic charging of electrode particles. Both profiles with (solid lines) and without (dashed lines) the mechanical-to-chemical coupling, namely the SED effect, are given: (a) Typical concentration profile in a spherical $LiMn_2O_4$ particle [50]; (b) Typical concentration profile, normalized into the SOC, in a spherical LiC_6 particle [25]; (c) Concentration profile in a Li/Si nanowire when galvanostatically lithiated to the half-charged state [68]. Figures reproduced with permission.

rection of diffusion. Using Eq. (10) and the elasticity assumption, Hartbaradaran et al. [18] found a class of nonconventional solutions indicative of a surface locking instability. Simply speaking, as Li is inserted from the outer surface of an electrode, the magnitude of the biaxial stresses (compressive hence negative) near the surface increases and the diffusivity decreases accordingly (cf. Eq. (10)). If either the characteristic dimension of the electrode is sufficiently large or the charging rate is sufficiently high (or both), lithium atoms near the surface would not be able to move into the interior of the electrode because D^{Li} near the surface becomes too low. This effect would eventually result in a divergence in the concentration profile near the surface [18]. One experimental observation that is closely related to this physical picture is the self-limiting lithiation in crystalline nanowires [35]. There, significant retardation of lithiation diffusion into the core of the nanowires has been attributed to the stress-induced modulation of diffusivity in Eq. (10). Still, it is useful to bear in mind that in most situations the stresses are limited by the material's yield threshold and are reasonably low, such that the effect of Eq. (10) may be negligible. Therefore, most discussions in this review paper pertain to mechanical-to-chemical coupling only in the form of chemical potential shift as described in section 4.1. The effect of the coupling via activation barrier shift as given in Eq. (10) is not implied, unless explicitly specified otherwise.

4.3 Finite element implementation

One of the major numerical challenges in simulating the chemo-mechanical coupling as depicted in section 4.1 is associated with the gradient of the hydrostatic stress (i.e., $\partial\sigma_m/\partial X_J$) when a finite element (FE) method is used. Since $\partial\sigma_m/\partial X_J \propto \partial\varepsilon_m^e/\partial X_J$, either the strain gradient or the stress gradient itself has to be calculated numerically. Tang et al. [86] used a finite difference method to analyze the diffusion-stress coupling in olivine electrodes and successfully reproduced the phase transformation characteristics observed in experiments. The benefit of using a finite difference scheme is that one can automatically capture the 2nd-order deformation gradient by using appropriate discretized gradient operators. The finite element method, however, is more valuable if geometric shapes other than rectangles are involved.

However, when a linear interpolation function is used with a finite element, the information of strain gradient is lost since the diagonal terms of the interpolator's spatial Hessian are always zero. One remedy is to use elements with high-order polynomials as the interpolation functions. Another strategy is to compute the 2nd order deformation gradient by fitting to nodal displacements across several adjacent elements, instead of relying only on the nodal values of one specific element under consideration [94]. These methods fall into the category of irreducible finite element methods.

Bower and Guduru [91] and Gao et al. [68] independently proposed methods that leverage the concept of mixed finite elements [95] to simulate the diffusion/deformation two–way coupling. Instead of using only the deformation and concentration of the diffusion species as nodal variables, the hydrostatic stress σ_m [68] or the Li chemical potential [91] can also be treated as a redundant degree of freedom, thereby automatically resolve the relevant gradient needed by Fick's law (Eq. (8)). For example, one can use σ_m as the redundant variable and then constrain it by [68]

$$\int_V \left[\frac{\det(\mathbf{F})}{\det(\mathbf{F}^{SF})} - 1 - \frac{\sigma_m}{K}\right]\delta\sigma_m dV = 0. \tag{11}$$

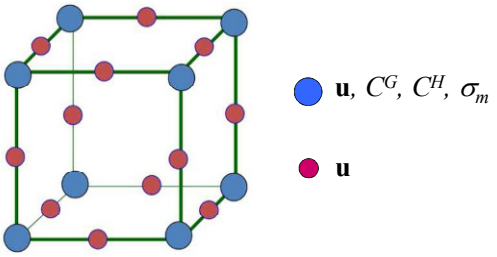

Fig. 10. The mixed finite element used to calculate deformation/interdiffusion coupling in alloy-based electrodes. 2nd order isoparametric shape functions are used for displacement and linear isoparametric shape functions are used for concentration and pressure. The corner nodes have displacement, concentration and hydrostatic stress DOF and the edge nodes only have displacement DOF. Reproduced from Ref. [17] with permission.

This relation is simply the variational form of the hydrostatic part of Hook's law. Using the 20-node mixed element as shown in Fig. 10, Gao and Zhou solved a range of problems such as the relaxation of stress by interdiffusion [17] and the effect of lithiation-induced softening on SED [75]. The numerical framework independently proposed by Bower et al. [91] is based on a similar principle, although the redundant variable chosen is Li chemical potential and the element used is linear. Both methods [17, 91] are reported to be highly efficient and stable.

5. Fracture mechanics

5.1 Models based on maximum tensile stress and the total strain energy

Cheng et al. [48] considered a fracture initiation criterion in a spherical electrode that is based on equating the maximum tensile stress $\sigma^{\max}$ found in the electrode with the fracture strength σ_F of the electrode material, i.e.

$$\sigma^{\max} = \sigma_F. \tag{12}$$

In order to quantify the relative importance of surface kinetics and diffusion, they adopted the Biot number original used for thermal stress problems [96]. For spherical electrode particles with radius R, the Biot number is defined as $B = \left(k_a^{'} + k_c^{'}\right)R/\left(D_I c\right)$, where D_I is the diffusivity, c is the molar concentration, and $k_a^{'}$ and $k_c^{'}$ are the anodic and cathodic rate constants, respectively. When B is large, the surface reaction is fast compared to diffusion and vice versa when B is small. For both small and large B values, it is found that a high value of $(1-\nu)\sigma_F/E$ is desirable because, for the same charging conditions, a lower value of $(1-\nu)/E$ decreases $\sigma^{\max}$ while a higher σ_F signifies higher fracture resistance. This maximum-stress-based criterion is nevertheless incomplete, because it only relates to the nucleation of cracks but not the subsequent propagation [46]. Cracks, once formed, may not propagate if there is insufficient energy to create new fracture surfaces.

To quantify the likelihood for both crack initiation and for nucleated cracks to grow, Cheng et al. [46] later proposed a criterion that is essentially an electrochemical counterpart of Hasselman's thermal shock model [97]. This model [46] is based on the assumption that all the elastic energy associated with the diffusion-induced stresses (DIS) can be eventually transformed into effective surface energy and that the body is stress-free when cracks are arrested. Specifically, the total surface energy required for crack propagation is equal to the total elastic energy E_T, such that

$$E_T = 2AN\gamma_{eff}. \tag{13}$$

Here, A is the mean area over which N numbers of cracks will propagate in a sphere, and γ_{eff} is the effective surface energy. By using the total elastic energy E_T, Cheng et al. showed from Eq. (13) that the average crack area per unit electrode volume S_V is

$$S_V \approx 0.23\frac{1-\nu}{\gamma_{eff}E}\sigma_F^2. \tag{14}$$

It is reasoned that when S_V exceeds a critical value, the percolation path for electric current in the electrode will be destroyed, and the loss of electrical connectivity would lead to performance degradation.

The strain-energy-based criterion (Eq. (13)) is essentially a simplified version of the Griffith's criterion. The main advantage of such simplistic models as delineated in Refs. [46, 48] is the ease with which analytical solutions can be developed and used to study the main features of scaling laws that govern crack initiation and failure. Since lithiated silicon is highly ductile, such analytical solutions based on the linear elastic model may deviate significantly from realistic situations. Nonlinearity due to finite deformation and inelasticity usually necessitates more sophisticated models for fracture and numerical simulation. In terms of models based on the finite element analysis, primarily two methods are usually used by researchers to quantify fracture tendency. The first is based on the cohesive zone method and the second is based on the energy release rate.

5.2 Models based on cohesive zones

Cohesive models of fracture were originally developed to remove crack-tip stress singularity due to cohesive interactions [98] or plastic deformation [99]. This approach and the associated finite element framework called the cohesive finite element method (CFEM) have been used to simulate a wide range of fracture problems, including particle deboning, dynamic fracture and microstructural mechanisms of fracture [100-104]. Based on the concept of cohesive zones, Bhandakkar and Gao [105] developed an analytical model for crack nucleation in an initially crack-free stripe electrode during galvanostatic intercalation and deintercalation. For a periodic

array of cracks in a free-standing thin strip, they showed that there exists a critical length scale in the form of

$$H_{ft} = 13\left\{\frac{\Gamma(1-\nu)F^2D^2}{E(1+\nu)\Omega^2I^2}\right\}^{1/3} \tag{15}$$

where I is the surface current density, F is the Faraday's constant, D is the diffusivity, E is the Young's modulus, ν is the Poisson's ratio, Ω is the partial molar volume of Li, and Γ is the fracture energy which is the area under the traction-separation curve of the cohesive crack surface. When the characteristic dimension of the electrode, such as the thickness for the strip, is below H_{ft}, crack nucleation becomes impossible irrespective of the cohesive strength of the material. This is not because the peak stress in the electrode remains smaller than the cohesive strength, rather it is because the maximum surface separation within an emergent cohesive zone cannot reach the cohesive interaction range [105]. In this case, the localized deformation in the cohesive zone is fully recoverable once the diffusion-induced stresses are lowered. The overall trend given by Eq. (15) is consistent with that given by an analysis based on the maximum tensile stress [25, 48] and the total strain energy [46], although the scaling index [$H_{ft} \propto \Gamma^{1/3}D^{2/3}/\left(E^{1/3}I^{2/3}\right)$ here] is different from those given by the other two types of analysis. This difference is partly due to the difference in the failure criteria used and partly due to the difference in the geometric configurations and crack patterns considered. Specifically, the periodic crack patterns considered by Bhandakkar and Gao [105] involves interactions among adjacent cracks, while other analyses [25, 47, 48] mostly concern the nucleation and growth of isolated cracks. In realistic cases, whether the inter-crack interaction is important or not is likely dependent on the specific geometric configuration of the electrode.

Bower and Guduru [91] and Grandab and Shenoy [76] used the cohesive finite element method to analyze the fracture behavior of Li/Si electrodes. Both analyses consider the two-way coupling between diffusion and deformation, by using the mixed finite element method [106] or by calculating the pressure gradient from fields in adjacent elements [76]. It is found that the two-way coupling can lead to lithium accumulation at the crack tip [76], similar to the accumulation of hydrogen in hydrogen embrittlement problems. Such accumulations could have a significant impact on near-tip stress fields and, consequently, affect fracture [69]. The use of cohesive elements allows fracture propagation to be explicitly tracked with ease, compared with other propagation-tracking techniques such as crack-tip remeshing [107]. When significant plasticity is involved, however, care must be taken when using cohesive finite elements because the critical separation might be comparable or even larger than nano-sized features in the electrodes.

5.3 Fracture criteria based on energy release rate

Since lithiated silicon is highly ductile, fracture criteria based on the energy-release-rate seem to be a logical choice for fracture analyses. Hu et al. [108] used the energy release rate and the Griffith condition to study insertion-induced cracking in $LiFePO_4$ particles caused by the mismatch between different phases. Ryu et al. [109] proposed a framework for calculating the energy release rate J for cracks in Si nanowire electrodes and used the framework to study the size dependence of fracture. This theory nevertheless relies on the effective diffusivity D_{eff} as given by Eq. (9) and, therefore, is only applicable when the material deformation is elastic. In order to overcome this shortcoming, Gao and Zhou [69] developed a fully-coupled finite deformation theory for analyzing the coupled mechano-diffusional driving forces for fracture in electrode materials. They found that the standard form of J-integral as energy release is no longer path-independent when coupled mechano-diffusional driving forces are present. Instead, an area integral must be included to maintain path-independency, such that the energy release rate J is given by

$$J = \int_\Gamma \left[\phi\delta_{1J} - \sigma_{Ji}^{PK1}\left(\partial u_i/\partial X_1\right)\right]N_J d\Gamma_0 - \left(\int_{V_\Gamma} \mu^{Li}\frac{\partial C^{Li}}{\partial X_1}dA_0 - \int_\Gamma w^P\delta_{1J}N_J d\Gamma_0\right) \tag{16}$$

where Γ is the integration contour, V_Γ is the domain bounded by Γ, ϕ is the Lagrangian density of the Helmholtz free energy, σ_{Ji}^{PK1} is the first Piolo-Kirchoff stress, and w^P is the plastic potential. Here, the additional area integral [second term of Eq. (16)] is very similar to that found in hygrothermal [110] and dynamic [103, 111, 112] fracture problems.

By using the mixed finite element method and the J integral as given in Eq. (16), Gao and Zhou [69] showed that under loading, lithium accumulates at tips, leading to relaxation of the hydrostatic stress. When the material is linear elastic, it is found that this accumulation process does not affect in-plane stress fields or the stress intensity factor but increases the energy release rate. When the material is capable of deforming plastically, as is the case for lithiated Li/Si, it is found that global yielding (large scale yielding) provides a mechanism for stress relaxation which can significantly reduce the energy release rate. For a thin-film Li/Si electrode with a through-thickness surface crack of length a, they calculated the energy release rate J for the crack during the discharge process. The process they consider mimics the situation when a thin film is first charge to a SOC of Ξ_0, and then discharged galvanostatically. The amount of lithium extracted during such a discharge process is recorded as $\Delta\bar{\Xi}$. As shown in Fig. 11(a), the energy release rate J increases as more and more lithium is extracted. When J reaches the critical value J_{CR}, the surface crack would grow and penetrate the film. What is most interesting is the inflection points in the J- $\Delta\bar{\Xi}$ curves with higher values of Ξ_0. These inflection points are attributed to the onset of global yielding. When global yielding starts, stresses are relaxed by the plastic deformation and the energy

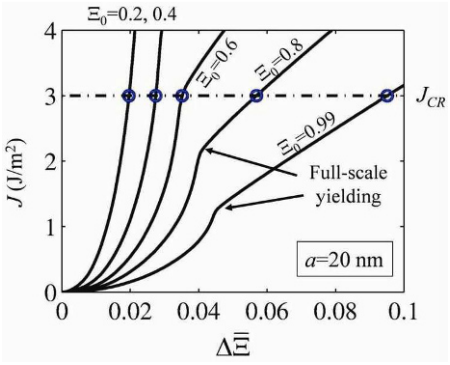

(a)

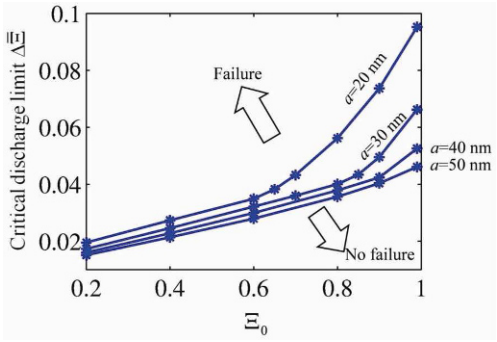

(b)

Fig. 11. (a) Dependence of energy release rate or driving force for fracture on discharge level $\Delta\bar{\Xi}$ and initial concentration Ξ_0 for a crack with a length of 20 nm in a thin film; (b) Design map showing the maximum extractable amount of lithium $\Delta\bar{\Xi}$ without crack growth as a function of initial SOC Ξ_0 for different pre-crack sizes. Reproduced from Ref. [69] with permission.

release rate is reduced relative to the levels in situations without plasticity. Since the elastic modulus and yield stress of Li/Si both decrease as Li concentration increases, full-scale yielding can be reached by the *J*- $\Delta\bar{\Xi}$ curves with higher Ξ_0 but not by those with lower Ξ_0 without first hitting the J=J_{CR} threshold. In other words, the driving force for fracture in thin-film electrodes can be lowered by operating thin-film electrodes at higher Li concentrations because such cycling regimens takes advantage of the effects of lithiation-induced softening or the brittle-ductile transition in failure mode.

Fig. 11(b) shows the maximum utilizable amount of Li (as measured by $\Delta\bar{\Xi}$) as a function of Ξ_0 when pre-cracks with different sizes are present in a thin film electrode. Here, $\bar{\Xi}\in\left(\Xi_0-\Delta\bar{\Xi}_{CR},\Xi_0\right)$ is the safe window in which the electrode can be operated without fracture. For each pre-crack length a, the corresponding $\Delta\bar{\Xi}_{CR}\sim\Xi_0$ curve delineates the boundary between the unsafe region (upper left) and the safe region (bottom right). In real thin-film electrodes, the smoothness of electrode surfaces is always limited by the manufacturing and operating conditions, such that the existence of surface defects is inevitable. It is concluded by Gao and Zhou from Fig. 11(b) that for the same operational capacity ($\Delta\bar{\Xi}$), a thin-film electrode is always more defect-tolerant when the charging/discharging regimen is designed such that the battery operates at higher concentration windows of $\bar{\Xi}\in\left(\Xi_0-\Delta\bar{\Xi}_{CR},\Xi_0\right)$.

It should be noted that as a fracture mechanics criterion, the Griffith condition generally does not apply to fatigue crack growth, while the failure of secondary battery electrodes can occur under static or cyclic loads (charge-discharge). For an electrode to last, however, it has to survive the first few cycles, during which electrode failure is mainly governed by fracture mechanics. Even when fatigue is important, analyses using relations such as the Paris law [113] generally require the calculation of fracture driving force in the form of K_I or J. Such fatigue analyses can be very challenging. Indeed, research in this regard has been carried out only for intercalation electrode materials [113], but not for alloy-based materials which may deform plastically. The fully-coupled theory of embodied in Eq. (16), therefore, can also be regarded as an essential part of future models for cyclic failure in alloy-based battery electrodes.

6. Electrode-electrolyte interaction and microstructural-level models

The models reviewed so far mainly concern the chemo-mechanical response of thin-film electrodes or isolated electrode particles. Such models focus on the processes in the solid domain of the electrode in which the electric potential is usually assumed to be a constant because of the high electric conductivity. In such treatments, transport in the electrolyte and on the electrolyte-electrode interface can be regarded as extrinsic, and the overall effect of this extrinsic process can be lumped into the boundary condition at the surface of the solid electrode domain. The boundary conditions typically considered include galvanostatic condition or potential static condition. For the former, surface influx is constant and predefined; for the latter, the electric potential of the cell is specified and the surface outflux of Li J^{Li} is governed by the well-known Butler-Volmer equation such that [25, 28, 88, 114, 115]

$$J^{Li}=\frac{i_0}{F}\left[\exp\left(\frac{\alpha_a F}{RT}\eta_s\right)-\exp\left(-\frac{\alpha_c F}{RT}\eta_s\right)\right] \tag{17}$$

where $i_0=i_0\left(C^+,C^{Li},T\right)$ is the exchange current density, a function of the Li concentration C^{Li} in the electrode particle at its surface, the concentration C^+ of Li^+ ions in the electrolyte, and temperature T. The parameters α_a and α_c are the transfer coefficients, and R is the ideal gas constant. Here $\eta_s=\Phi_s-\Phi_e-U\left(C^+,C^{Li},T\right)$ is known as the surface overpotential, where Φ_s is the potential at the electric particle surface, Φ_e is the electric potential in the eolectrolyte adjacent to the particle surface, and U is the open circuit potential (OCP). Usually, for potential-static charging conditions of a LiSi vs. Li metal half cell, the value of $V=\Phi_s-\Phi_e$ can be directly specified if the LiSi electrode is in the form of isolated particles or thin films, and the Li^+ ion concentration in the electrolyte is assumed to be a constant. Under these conditions,

J^{Li} can be uniquely determind from C^{Li} at the particle surface. Such an assumption is widely used to study potential-static charging processes of thin films and isolated particles (see e.g., Refs. [83, 84]).

In most Li-ion battery applications, however, the electrodes are made of neither isolated particles nor homogenous thin-films. Instead, the electrode is usually an aggregate of storage particles (e.g. LiSi particles), held together by a polymeric binder [116]. Often times, carbon-based additive is used to enhance the electric connectivity among active storage particles [117, 118]. The binder-particle microstructure is usually porous [116], so that electrolyte can penetrate inside and provide pathways for Li^+ transport. In these situations, Li^+ ion transport in the binder/electrolyte domain is no longer an extrinsic process as modeled in isolated particle models, and the spatial distribution of electric potential has to be explicitly considered together with the concentration and stress distribution [115].

As already mentioned, the Butler-Volmer kinetics provides a way to quantify the surface flux for isolated particles when the charging condition is potential-static, i.e., when the charging voltage $V = \Phi_s - \Phi_e$ is specified. For isolated particles charged under galvanostatic conditions, there is no need to explicitly consider the Butler-Volmer equation because the surface influx is directly stipulated by the system-wide electric current. For electrodes made of interacting particles, however, the Butler-Volmer equation, as well as the laws that govern transport inside the electrolyte domain, are needed even when the charging is galvanostatic. This is because in real galvanostatic experiments, it is the total current, not the current into each individual particle, that can be controlled and measured. Depending on the location and environment of each particle, the surface influx can be different [115].

There is no doubt that the complexity of models increases significantly when one goes from isolated particles to microstructures. Almost inevitably, simplifying assumptions and approximations are needed. The porous electrode theory [119, 120] is one of the earliest successful theories to reduce the complex microstructures of battery electrodes into a more tractable 1-D homogenized picture. This theory is essentially a mean-field theory, in which the electric potential, the Li concentration and flux, and the electric current are all homogenized into spatial-average quantities over a certain representative dimension. The microscopic transport equations in the electrolyte, active storage particle, electrolyte-electrode interface, along with the continuity equations of mass and electric field, are then averaged into governing equations for the homogenized variables.

Despite its powerfulness and wide application, the porous electrode theory by itself does not directly tackle the stresses in individual particles of the microstructure, because such stresses are microscopically local quantities instead of macroscopically homogenized ones. Christensen [114] proposed a pseudo-2D model which is essentially a multi-scale model that links the global solution of porous electrode theory to the microscopic response of an individual particle. The model is considered pseudo-2D because it entails two 1-D models in two different scales: an 1-D porous electrode model which is appropriate for cells with a collector-electrode-separator sandwich structure, and an 1-D diffusion/deformation coupling model of spherical-shaped electrode particles for which the radial coordinate is taken as the only relevant spatial dimension. The scale linking is achieved by utilizing the pore-wall flux computed in the porous electrode material, as a boundary condition at the surface of the microscopic single particle domain. The particle domain equation is in turn solved to yield the lithium concentration at the spherical surface. Through feeding of this surface concentration back into the porous electrode model via the Butler-Volmer kinetics [cf. Eq. (17)], the two domains are connected to allow calculation of stresses and fracture tendency in active storage particles.

Beside the multi-scale technique proposed by Christensen [114], models that directly simulate the coupling between electrochemistry and mechanical deformation at the microscopic level have also been developed. Garcia et al. [117, 118] studied the effect of microstructures on transport process and stress buildup using such a bottom-up approach by leveraging the finite element method. In terms of cathode macrostructures, they found that battery performance could be improved by controlling the transport paths to the back of the positive porous electrode, maximizing the surface area for intercalating lithium ions, and carefully controlling the spatial distribution and particle size of active material [117]. They also discussed the potential benefit of using interpenetrating electrode architectures, which has highly percolating particle distributions with short diffusion distances. The original models developed by Garcia et al. only considered the one-way coupling of diffusion-induced stresses. It was later augmented by Purkayastha and McMeeking, who introduced the effect of stress gradient on diffusion as well [115].

One of the main advantages of the bottom-up approaches, which start from the microscopic level up to higher levels, is that such approaches allow non-spherical particle shapes. Even when the particles are spherical, the quasi-2D model is based on the assumption that concentration and stress fields in the particle are spherically symmetric. The reality is generally not the case [91, 115], as shown in Fig. 12. The bottom-up approaches are nevertheless computationally expensive. Indeed, most of such studies are 2-D [115, 117, 118]. When 3-D representations are sought, the microstructure is usually modeled with a very small number of particles in a representative unit cell that is repeated using periodic boundary conditions (see, e.g., Ref. [106]).

7. Concluding remarks

Miniaturization has shown to be an effective means to develop electrodes for the next generation high-capacity and high-performance rechargeable batteries. The improvement of nano-sized Li-alloy electrode materials requires a fundamental

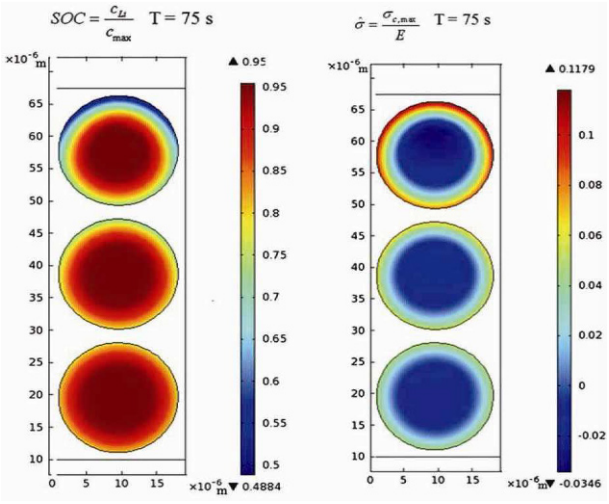

(a) (b)

Fig. 12. Contour plots of the maximum circumferential stress and SOC in a microstructure consisting of a row of three spherical particles at a charging time of 75 s. The stress and SOC in each particle is different, and the fields are not spherically symmetric in each particle. Reproduced from Ref. [115] with permission.

understanding of the chemo-mechanical characteristics of the coupled chemical-mechanical processes associated with the operation of batteries. While stress buildup associated with lithiation and delithiation bears certain resemblance to the development of thermo-stresses, a phenomenon better studied and relatively well-understood, the multiphysics processes in alloy-based electrodes are much more complex, challenging and intriguing. The reasons are not only because much larger deformations are involved, but also because the processes entail two-way coupling between diffusion and deformation, nonlinearity and chemical reaction. This richness of physics presents opportunities for interdisciplinary research to the solid mechanics, physics, chemistry, and materials communities. While the issues are challenging, the new phenomena are both theoretically interesting and practically important.

We have attempted to provide a review of the background, issues and latest research on the mechanical aspects of alloy-based anodes, especially those based on the Li/Si alloy, for Li-ion batteries. The coupling between diffusion and stress is two-way and the strength of the mechanical-to-chemical coupling in Li/Si is much stronger that what has been known in other electrode materials such as intercalation cathode materials (e.g., $LiFePO_4$) and carbonaceous anode materials (e.g., LiC_6). The diffusion-induced large deformations have been analyzed through Lee-type decompositions. Analyses have shown that lithiation-induced softening in terms of both the elastic modulus and the yield stress plays a very important role in determining the response of alloy electrodes. Such analyses necessitate realistic models that account for the relevant physics and special techniques. As one result of research heretofore, methods such as the mixed finite element method has been developed and used.

All models and analyses for alloy-based electrode materials ultimately have a common goal: to improve the performance of batteries in terms of capacity, cyclability, and power density. The mitigation of cycling-induced mechanical fracture and property degradation is generally regarded the foremost issue. The fracture models reviewed in section V share this common aim. On the other hand, experiments also show that besides fracture, alloy-based electrodes may also fail due to the formation and coalescence of internal voids [7]. Such failure by voiding, although potentially important, has been given much less attention than the failure by brittle or ductile fracture. Future research in this regard is considered highly relevant and important by the authors.

On the other hand, most research on the mechanical issues of battery electrodes have focused on the stresses and fracture in the electrode material itself. Relatively less research has been carried out to consider the effects of the solid-electrolyte interphase (SEI), a layer that forms on the surface of electrodes [121]. This is partly due to a lack of experimental data on the mechanical properties of SEI. Nevertheless, studies by Wu et al. [5] indicates that the interaction between the SEI and the electrode material may significantly affect battery cyclability. Understanding of the implications of SEI on the stresses and failure tendency is probably the most important missing link between the current mechanical models and a more comprehensive understanding of the interplays among different factors in battery operation.

Finally, it is important to point out that ultimately the design of battery electrodes must reach the macroscopic size scale. As such, it is recognized that the microstructures of electrodes consist of not only the active particles or films, but also a binder and a network of pores. The design of microstructures account for the essential multiphysics processes and the hierarchical nature of the materials is yet another area with significant research needs.

Acknowledgement

Support from the National Research Foundation of Korea through WCU Grant No. R31-2009-000-10083-0 is acknowledged.

References

[1] L. Y. Beaulieu, T. D. Hatchard, A. Bonakdarpour, M. D. Fleischauer and J. R. Dahn, Reaction of Li with alloy thin films studied by in situ AFM, *Journal of the Electrochemical Society*, 150 (2003) A1457-A1464.

[2] Y. Qi, H. B. Guo, L.G. Hector and A. Timmons, Threefold increase in the young's modulus of graphite negative electrode during lithium intercalation, *Journal of the Electrochemical Society*, 157 (2010) A558-A566.

[3] D. Larcher, S. Beattie, M. Morcrette, K. Edstroem, J. C. Jumas and J. M. Tarascon, Recent findings and prospects in

the field of pure metals as negative electrodes for Li-ion batteries, *Journal of Materials Chemistry*, 17 (2007) 3759-3772.

[4] H. Wu, G. Zheng, N. Liu, T. J. Carney, Y. Yang and Y. Cui, Engineering empty space between Si nanoparticles for lithium-ion battery anodes, *Nano Lett*, 12 (2012) 904-909.

[5] H. Wu, G. Chan, J. W. Choi, I. Ryu, Y. Yao, M. T. McDowell, S. W. Lee, A. Jackson, Y. Yang, L. B. Hu and Y. Cui, Stable cycling of double-walled silicon nanotube battery anodes through solid-electrolyte interphase control, *Nature Nanotechnology*, 7 (2012) 309-314.

[6] Y. Yao, M. T. McDowell, I. Ryu, H. Wu, N. Liu, L. Hu, W. D. Nix and Y. Cui, Interconnected silicon hollow nanospheres for lithium-ion battery anodes with long cycle life, *Nano Lett*, 11 (2011) 2949-2954.

[7] L. B. Hu, H. Wu, Y. F. Gao, A. Y. Cao, H. B. Li, J. McDough, X. Xie, M. Zhou and Y. Cui, Silicon-carbon nanotube coaxial sponge as Li-ion anodes with high areal capacity, *Advanced Energy Materials*, 1 (2011) 523-527.

[8] C. K. Chan, H. Peng, G. Liu, K. McIlwrath, X. F. Zhang, R. A. Huggins and Y. Cui, High-performance lithium battery anodes using silicon nanowires, *Nat Nanotechnol*, 3 (2008) 31-35.

[9] L. F. Cui, R. Ruffo, C. K. Chan, H. L. Peng and Y. Cui, Crystalline-amorphous core-shell silicon nanowires for high capacity and high current battery electrodes, *Nano Letters*, 9 (2009) 491-495.

[10] T. Song, J. Xia, J. H. Lee, D. H. Lee, M. S. Kwon, J. M. Choi, J. Wu, S. K. Doo, H. Chang, W. I. Park, D. S. Zang, H. Kim, Y. Huang, K. C. Hwang, J. A. Rogers and U. Paik, Arrays of sealed silicon nanotubes as anodes for lithium ion batteries, *Nano Lett*, 10 (2010) 1710-1716.

[11] A. Magasinski, P. Dixon, B. Hertzberg, A. Kvit, J. Ayala and G. Yushin, High-performance lithium-ion anodes using a hierarchical bottom-up approach, *Nature Materials*, 9 (2010) 353-358.

[12] L. Y. Beaulieu, K. W. Eberman, R. L. Turner, L. J. Krause and J. R. Dahn, Colossal reversible volume changes in lithium alloys, *Electrochemical and Solid State Letters*, 4 (2001) A137-A140.

[13] J. W. Choi, J. McDonough, S. Jeong, J. S. Yoo, C. K. Chan and Y. Cui, Stepwise nanopore evolution in one-dimensional nanostructures, *Nano Letters*, 10 (2010) 1409-1413.

[14] V. A. Sethuraman, M. J. Chon, M. Shimshak, V. Srinivasan and P. R. Guduru, In situ measurements of stress evolution in silicon thin films during electrochemical lithiation and delithiation, *Journal of Power Sources*, 195 (2010) 5062-5066.

[15] A. F. Bower, P. R. Guduru and V. A. Sethuraman, A finite strain model of stress, diffusion, plastic flow, and electrochemical reactions in a lithium-ion half-cell, *Journal of the Mechanics and Physics of Solids*, 59 (2011) 804-828.

[16] K. J. Zhao, M. Pharr, J. J. Vlassak and Z. G. Suo, Fracture of electrodes in lithium-ion batteries caused by fast charging, *Journal of Applied Physics*, 108 (2010) 073517.

[17] Y. F. Gao, M. Cho and M. Zhou, Stress relaxation through interdiffusion in amorphous lithium alloy electrodes, *Journal of the Mechanics and Physics of Solids*, 61 (2013) 579-596.

[18] H. Haftbaradaran, H. J. Gao and W. A. Curtin, A surface locking instability for atomic intercalation into a solid electrode, *Applied Physics Letters*, 96 (2010).

[19] Y. T. Cheng and M. W. Verbrugge, The influence of surface mechanics on diffusion induced stresses within spherical nanoparticles, *Journal of Applied Physics*, 104 (2008).

[20] L. Anand, A Cahn-Hilliard-type theory for species diffusion coupled with large elastic-plastic deformations, *Journal of the Mechanics and Physics of Solids*, 60 (2012) 1983-2002.

[21] I. Ryu, J. W. Choi, Y. Cui and W. D. Nix, Size-dependent fracture of Si nanowire battery anodes, *Journal of the Mechanics and Physics of Solids*, 59 (2011) 1717-1730.

[22] S. Huang and T. Zhu, Atomistic mechanisms of lithium insertion in amorphous silicon, *Journal of Power Sources*, 196 (2011) 3664-3668.

[23] V. Chevrier, J. Zwanziger and J. Dahn, First principles study of Li-Si crystalline phases: Charge transfer, electronic structure, and lattice vibrations, *Journal of Alloys and Compounds*, 496 (2010) 25-36.

[24] V. L. Chevrier and J. R. Dahn, First principles model of amorphous silicon lithiation, *Journal of the Electrochemical Society*, 156 (2009) A454-A458.

[25] J. Christensen and J. Newman, Stress generation and fracture in lithium insertion materials, *Journal of Solid State Electrochemistry*, 10 (2006) 293-319.

[26] P. Limthongkul, Y. I. Jang, N. J. Dudney and Y. M. Chiang, Electrochemically-driven solid-state amorphization in lithium-silicon alloys and implications for lithium storage, *Acta Materialia*, 51 (2003) 1103-1113.

[27] P. Limthongkul, Y. I. Jang, N. J. Dudney and Y. M. Chiang, Electrochemically-driven solid-state amorphization in lithium-metal anodes, *Journal of Power Sources*, 119 (2003) 604-609.

[28] M. Pharr, K. J. Zhao, X. W. Wang, Z. G. Suo and J. J. Vlassak, Kinetics of initial lithiation of crystalline silicon electrodes of lithium-ion batteries, *Nano Letters*, 12 (2012) 5039-5047.

[29] X. H. Liu, L. Zhong, S. Huang, S. X. Mao, T. Zhu and J. Y. Huang, Size-dependent fracture of silicon nanoparticles during lithiation, *Acs Nano*, 6 (2012) 1522-1531.

[30] X. H. Liu, H. Zheng, L. Zhong, S. Huang, K. Karki, L. Q. Zhang, Y. Liu, A. Kushima, W. T. Liang, J. W. Wang, J. H. Cho, E. Epstein, S. A. Dayeh, S. T. Picraux, T. Zhu, J. Li, J. P. Sullivan, J. Cumings, C. Wang, S. X. Mao, Z. Z. Ye, S. Zhang and J. Y. Huang, Anisotropic swelling and fracture of silicon nanowires during lithiation, *Nano Lett*, 11 (2011) 3312-3318.

[31] X. H. Liu and J. Y. Huang, In situ TEM electrochemistry of anode materials in lithium ion batteries, *Energy & Environmental Science*, 4 (2011) 3844-3860.

[32] X. H. Liu, J. W. Wang, S. Huang, F. F. Fan, X. Huang, Y. Liu, S. Krylyuk, J. Yoo, S. A. Dayeh, A. V. Davydov, S. X. Mao, S. T. Picraux, S. L. Zhang, J. Li, T. Zhu and J. Y. Huang, In situ atomic-scale imaging of electrochemical lithiation in silicon, *Nature Nanotechnology*, 7 (2012) 749-756.

[33] S. W. Lee, M. T. McDowell, J. W. Choi and Y. Cui, Anomalous shape changes of silicon nanopillars by electrochemical lithiation, *Nano Lett*, 11 (2011) 3034-3039.

[34] H. Yang, S. Huang, X. Huang, F. F. Fan, W. T. Liang, X. H. Liu, L. Q. Chen, J. Y. Huang, J. Li, T. Zhu and S. L. Zhang, Orientation-dependent interfacial mobility governs the anisotropic swelling in lithiated silicon nanowires, *Nano Letters*, 12 (2012) 1953-1958.

[35] X. H. Liu, F. F. Fan, H. Yang, S. L. Zhang, J. Y. Huang and T. Zhu, Self-limiting lithiation in silicon nanowires, (2013) DOI: 10.1021/nn305282d.

[36] S. W. Lee, M. T. McDowell, L. A. Berla, W. D. Nix and Y. Cui, Fracture of crystalline silicon nanopillars during electrochemical lithium insertion, *Proceedings of the National Academy of Sciences of the United States of America*, 109 (2012) 4080-4085.

[37] Z. W. Cui, F. Gao and J. M. Qu, A finite deformation stress-dependent chemical potential and its applications to lithium ion batteries, *Journal of the Mechanics and Physics of Solids*, 60 (2012) 1280-1295.

[38] K. J. Zhao, M. Pharr, S. Q. Cai, J. J. Vlassak and Z. G. Suo, Large plastic deformation in high-capacity lithium-ion batteries caused by charge and discharge, *Journal of the American Ceramic Society*, 94 (2011) S226-S235.

[39] S. Prussin, The generation and distribution of dislocations by solute diffusion, *Journal of Applied Physics*, 32 (1961) 1876.

[40] J. C. M. Li, Physical-chemistry of some microstructural phenomena, *Metallurgical Transactions a-Physical Metallurgy and Materials Science*, 9 (1978) 1353-1380.

[41] S. B. Lee, W. L. Wang and J. R. Chen, Diffusion-induced stresses in a hollow cylinder: Constant surface stresses, *Materials Chemistry and Physics*, 64 (2000) 123-130.

[42] W. L. Wang, S. Lee and J. R. Chen, Effect of chemical stress on diffusion in a hollow cylinder, *Journal of Applied Physics*, 91 (2002) 9584-9590.

[43] S. C. Ko, S. Lee and Y. T. Chou, Chemical stresses in a square sandwich composite, *Materials Science and Engineering a-Structural Materials Properties Microstructure and Processing*, 409 (2005) 145-152.

[44] F. Q. Yang, Interaction between diffusion and chemical stresses, *Materials Science and Engineering a-Structural Materials Properties Microstructure and Processing*, 409 (2005) 153-159.

[45] Y. T. Cheng and M. W. Verbrugge, Evolution of stress within a spherical insertion electrode particle under potentiostatic and galvanostatic operation, *Journal of Power Sources*, 190 (2009) 453-460.

[46] Y. T. Cheng and M. W. Verbrugge, Application of hasselman's crack propagation model to insertion electrodes, *Electrochemical and Solid State Letters*, 13 (2010) A128-A131.

[47] R. Deshpande, Y. T. Cheng and M. W. Verbrugge, Modeling diffusion-induced stress in nanowire electrode structures, *Journal of Power Sources*, 195 (2010) 5081-5088.

[48] Y. T. Cheng and M. W. Verbrugge, Diffusion-induced stress, interfacial charge transfer, and criteria for avoiding crack initiation of electrode particles, *Journal of the Electrochemical Society*, 157 (2010) A508-A516.

[49] J. Christensen and J. Newman, A mathematical model of stress generation and fracture in lithium manganese oxide, *Journal of the Electrochemical Society*, 153 (2006) A1019-A1030.

[50] X. Zhang, W. Shyy and A. M. Sastry, Numerical simulation of intercalation-induced stress in Li-ion battery electrode particles, *Journal of the Electrochemical Society*, 154 (2007) A910.

[51] N. A. Liu, L. B. Hu, M. T. McDowell, A. Jackson and Y. Cui, Prelithiated silicon nanowires as an anode for lithium ion batteries, *Acs Nano*, 5 (2011) 6487-6493.

[52] L. Y. Beaulieu, S. D. Beattie, T. D. Hatchard and J. R. Dahn, The electrochemical reaction of lithium with tin studied by in situ AFM, *Journal of the Electrochemical Society*, 150 (2003) A419-A424.

[53] X. Xiao, P. Liu, M. W. Verbrugge, H. Haftbaradaran and H. Gao, Improved cycling stability of silicon thin film electrodes through patterning for high energy density lithium batteries, *Journal of Power Sources*, 196 (2011) 1409-1416.

[54] J. C. Li, A. K. Dozier, Y. C. Li, F. Q. Yang and Y. T. Cheng, Crack pattern formation in thin film lithium-ion battery electrodes, *Journal of the Electrochemical Society*, 158 (2011) A689-A694.

[55] B. Laforge, L. Levan-Jodin, R. Salot and A. Billard, Study of germanium as electrode in thin-film battery, *Journal of the Electrochemical Society*, 155 (2008) A181-A188.

[56] M. Winter and J. O. Besenhard, Electrochemical lithiation of tin and tin-based intermetallics and composites, *Electrochimica Acta*, 45 (1999) 31-50.

[57] K. Leung and Z. Neda, Pattern formation and selection in quasistatic fracture, *Physical Review Letters*, 85 (2000) 662-665.

[58] D. Gross, T. Seelig and SpringerLink (Online service), in: Mechanical engineering series,, Springer,, Berlin ; New York (2006) xii, 319.

[59] S. K. Soni, B. W. Sheldon, X. C. Xiao, M. W. Verbrugge, D. Ahn, H. Haftbaradaran and H. J. Gao, Stress mitigation during the lithiation of patterned amorphous Si islands, *Journal of the Electrochemical Society*, 159 (2012) A38-A43.

[60] H. Haftbaradaran, S. K. Soni, B. W. Sheldon, X. C. Xiao and H. J. Gao, Modified stoney equation for patterned thin film electrodes on substrates in the presence of interfacial sliding, *Journal of Applied Mechanics-Transactions of the Asme*, 79 (2012).

[61] H. Haftbaradaran, X. C. Xiao, M. W. Verbrugge and H. J. Gao, Method to deduce the critical size for interfacial delamination of patterned electrode structures and application to lithiation of thin-film silicon islands, *Journal of Power Sources*, 206 (2012) 357-366.

[62] R. F. Cook, Strength and sharp contact fracture of silicon, *Journal of Materials Science*, 41 (2006) 841-872.

[63] V. A. Sethuraman, M. J. Chon, M. Shimshak, N. Van Winkle and P. R. Guduru, In situ measurement of biaxial modulus of Si anode for Li-ion batteries, *Electrochemistry*

Communications, 12 (2010) 1614-1617.

[64] G. G. Stoney, The tension of metallic films deposited by electrolysis, *Proceedings of the Royal Society of London Series a-Containing Papers of a Mathematical and Physical Character*, 82 (1909) 172-175.

[65] K. J. Zhao, W. L. Wang, J. Gregoire, M. Pharr, Z. G. Suo, J. J. Vlassak and E. Kaxiras, Lithium-assisted plastic deformation of silicon electrodes in lithium-ion batteries: A first-principles theoretical study, *Nano Letters*, 11 (2011) 2962-2967.

[66] B. Hertzberg, J. Benson and G. Yushin, Ex-situ depth-sensing indentation measurements of electrochemically produced Si-Li alloy films, *Electrochemistry Communications*, 13 (2011) 818-821.

[67] V. B. Shenoy, P. Johari and Y. Qi, Elastic softening of amorphous and crystalline Li-Si Phases with increasing Li concentration: A first-principles study, *Journal of Power Sources*, 195 (2010) 6825-6830.

[68] Y. F. Gao and M. Zhou, Strong stress-enhanced diffusion in amorphous lithium alloy nanowire electrodes, *Journal of Applied Physics*, 109 (2011) 014310.

[69] Y. F. Gao and M. Zhou, Coupled mechano-diffusional driving forces for fracture in electrode materials, *Journal of Power Sources*, 230 (2013) 176-193.

[70] L. Brassart and Z. G. Suo, Reactive flow in solids, *Journal of the Mechanics and Physics of Solids*, 61 (2013) 61-77.

[71] L. Brassart and Z. G. Suo, Reactive flow in large-deformation electrodes of lithium-ion batteries, *International Journal of Applied Mechanics*, 4 (2012).

[72] K. J. Zhao, M. Pharr, J. J. Vlassak and Z. G. Suo, Inelastic hosts as electrodes for high-capacity lithium-ion batteries, *Journal of Applied Physics*, 109 (2011).

[73] C. H. Wu, The role of Eshelby stress in composition-generated and stress-assisted diffusion, *Journal of the Mechanics and Physics of Solids*, 49 (2001) 1771-1794.

[74] E. H. Lee, Elastic-plastic deformation at finite strains, *Journal of Applied Mechanics*, 36 (1969) 1.

[75] Y. F. Gao and M. Zhou, Strong dependency of lithium diffusion on mechanical constraints in high-capacity Li-ion battery electrodes, *Acta Mechanica Sinica*, 28 (2012) 1068-1077.

[76] R. Grantab and V. B. Shenoy, Pressure-gradient dependent diffusion and crack propagation in lithiated silicon nanowires, *Journal of the Electrochemical Society*, 159 (2012) A584-A591.

[77] M. W. Verbrugge and Y. T. Cheng, Stress and strain-energy distributions within diffusion-controlled insertion-electrode particles subjected to periodic potential excitations, *Journal of the Electrochemical Society*, 156 (2009) A927-A937.

[78] R. Deshpande, Y. T. Cheng, M. W. Verbrugge and A. Timmons, Diffusion induced stresses and strain energy in a phase-transforming spherical electrode particle, *Journal of the Electrochemical Society*, 158 (2011) A718-A724.

[79] R. Deshpande, Y. Qi and Y. T. Cheng, Effects of concentration-dependent elastic modulus on diffusion-induced stresses for battery applications, *Journal of the Electrochemical Society*, 157 (2010) A967-A971.

[80] T. K. Bhandakkar and H. T. Johnson, Diffusion induced stresses in buckling battery electrodes, *Journal of the Mechanics and Physics of Solids*, 60 (2012) 1103-1121.

[81] B. W. Sheldon, S. K. Soni, X. C. Xiao and Y. Qi, Stress contributions to solution thermodynamics in Li-Si alloys, *Electrochemical and Solid State Letters*, 15 (2012) A9-A11.

[82] R. Chandrasekaran, A. Magasinski, G. Yushin and T. F. Fuller, Analysis of lithium insertion/deinsertion in a silicon electrode particle at room temperature, *Journal of the Electrochemical Society*, 157 (2010) A1139-A1151.

[83] S. Golmon, K. Maute, S. H. Lee and M. L. Dunn, Stress generation in silicon particles during lithium insertion, *Applied Physics Letters*, 97 (2010).

[84] J. C. Li, X. C. Xiao, F. Q. Yang, M. W. Verbrugge and Y. T. Cheng, Potentiostatic intermittent titration technique for electrodes governed by diffusion and interfacial reaction, *Journal of Physical Chemistry C*, 116 (2012) 1472-1478.

[85] M. Tang, W. C. Carter, J. F. Belak and Y. M. Chiang, Modeling the competing phase transition pathways in nanoscale olivine electrodes, *Electrochimica Acta*, 56 (2010) 969-976.

[86] M. Tang, W. C. Carter and Y. M. Chiang, Electrochemically driven phase transitions in insertion electrodes or lithium-ion batteries: Examples in lithium metal phosphate olivines, *Annual Review of Materials Research, Vol 40*, 40 (2010) 501-529.

[87] M. Tang, H. Y. Huang, N. Meethong, Y. H. Kao, W. C. Carter and Y. M. Chiang, Model for the particle size, overpotential, and strain dependence of phase transition pathways in storage electrodes: Application to nanoscale olivines, *Chemistry of Materials*, 21 (2009) 1557-1571.

[88] R. Purkayastha and R. M. McMeeking, A linearized model for lithium ion batteries and maps for their performance and failure, *Journal of Applied Mechanics-Transactions of the Asme*, 79 (2012) 031021.

[89] F. C. Larche and J. W. Cahn, The interactions of composition and stress in crystalline solids, *Acta Metallurgica*, 33 (1985) 331-357.

[90] B. Yang, Y. P. He, J. Irsa, C. A. Lundgren, J. B. Ratchford and Y. P. Zhao, Effects of composition-dependent modulus, finite concentration and boundary constraint on Li-ion diffusion and stresses in a bilayer Cu-coated Si nano-anode, *Journal of Power Sources*, 204 (2012) 168-176.

[91] A. F. Bower and P. R. Guduru, A simple finite element model of diffusion, finite deformation, plasticity and fracture in lithium ion insertion electrode materials, *Modelling and Simulation in Materials Science and Engineering*, 20 (2012) 045004.

[92] G. G. Botte and R. E. White, Modeling lithium intercalation in a porous carbon electrode, *Journal of the Electrochemical Society*, 148 (2001) A54-A66.

[93] H. Haftbaradaran, J. Song, W. A. Curtin and H. J. Gao, Continuum and atomistic models of strongly coupled diffusion, stress, and solute concentration, *Journal of Power Sources*, 196 (2011) 361-370.

[94] R. K. Abu Al-Rub and G. Z. Voyiadjis, A direct finite element implementation of the gradient-dependent theory, *In-*

ternational Journal for Numerical Methods in Engineering, 63 (2005) 603-629.

[95] O. C. Zienkiewicz, R. L. Taylor and J. Z. Zhu, *The finite element method its basis and fundamentals*, 6th ed., *Elsevier Butterworth-Heinemann*, Amsterdam; London (2005).

[96] R. B. Hetnarski and M. R. Eslami, *Thermal stresses -- Advanced theory and applications*, *Springer*, Dordrecht; London (2008).

[97] D. P. H. Hasselman, Elastic energy at fracture and surface energy as design criteria for thermal shock, *Journal of the American Ceramic Society*, 46 (1963) 535-540.

[98] G. Barenblatt, The formation of equilibrium cracks during brittle fracture, *Journal of Applied Mathematics and Mechanics*, 23 (1959) 622-636.

[99] D. S. Dugdale, Yielding of steel sheets containing slits, *Journal of the Mechanics and Physics of Solids*, 8 (1960) 100-104.

[100] A. Needleman, A continuum model for void nucleation by inclusion debonding, *Journal of Applied Mechanics-Transactions of the Asme*, 54 (1987) 525-531.

[101] G. T. Camacho and M. Ortiz, Computational modelling of impact damage in brittle materials, *International Journal of Solids and Structures*, 33 (1996) 2899-2938.

[102] J. Zhai, V. Tomar and M. Zhou, Micromechanical simulation of dynamic fracture using the cohesive finite element method, *Journal of Engineering Materials and Technology-Transactions of the Asme*, 126 (2004) 179-191.

[103] Y. Li and M. Zhou, Prediction of fracture toughness of ceramic composites as function of microstructure: I. numerical simulations, *Journal of the Mechanics and Physics of Solids*, 61 (2013) 472-488.

[104] A. Barua and M. Zhou, A lagrangian framework for analyzing microstructural level response of polymer-bonded explosives, *Modelling and Simulation in Materials Science and Engineering*, 19 (2011).

[105] T. K. Bhandakkar and H. J. Gao, Cohesive modeling of crack nucleation under diffusion induced stresses in a thin strip: Implications on the critical size for flaw tolerant battery electrodes, *International Journal of Solids and Structures*, 47 (2010) 1424-1434.

[106] F. Zhang, A. F. Bower and W. A. Curtin, Finite element implementation of a kinetic model of dynamic strain aging in aluminum-magnesium alloys, *International Journal for Numerical Methods in Engineering*, 86 (2011) 70-92.

[107] P. O. Bouchard, F. Bay, Y. Chastel and I. Tovena, Crack propagation modelling using an advanced remeshing technique, *Computer Methods in Applied Mechanics and Engineering*, 189 (2000) 723-742.

[108] Y. H. Hu, X. H. Zhao and Z. G. Suo, Averting cracks caused by insertion reaction in lithium-ion batteries, *Journal of Materials Research*, 25 (2010) 1007-1010.

[109] P. Sofronis and J. Lufrano, Interaction of local elastoplasticity with hydrogen: embrittlement effects, *Materials Science and Engineering a-Structural Materials Properties Microstructure and Processing*, 260 (1999) 41-47.

[110] X. H. Chen, Coupled hygro-thermo-viscoelastic fracture theory, *International Journal of Fracture*, 148 (2007) 47-55.

[111] M. Zhou, G. Ravichandran and A. J. Rosakis, Dynamically propagating shear bands in impact-loaded prenotched plates .2. Numerical simulations, *Journal of the Mechanics and Physics of Solids*, 44 (1996) 1007.

[112] T. Nakamura, C. F. Shih and L. B. Freund, Computational methods based on an energy integral in dynamic fracture, *International Journal of Fracture*, 27 (1985) 229-243.

[113] R. Deshpande, M. Verbrugge, Y. T. Cheng, J. Wang and P. Liu, Battery cycle life prediction with coupled chemical degradation and fatigue mechanics, *Journal of the Electrochemical Society*, 159 (2012) A1730-A1738.

[114] J. Christensen, Modeling diffusion-induced stress in Li-ion cells with porous electrodes, *Journal of the Electrochemical Society*, 157 (2010) A366-A380.

[115] R. T. Purkayastha and R. M. McMeeking, An integrated 2-D model of a lithium ion battery: the effect of material parameters and morphology on storage particle stress, *Computational Mechanics*, 50 (2012) 209-227.

[116] T. Hutzenlaub, S. Thiele, R. Zengerle and C. Ziegler, Three-dimensional reconstruction of a LiCoO2 Li-ion battery cathode, *Electrochemical and Solid State Letters*, 15 (2012) A33-A36.

[117] R. E. Garcia, Y. M. Chiang, W. C. Carter, P. Limthongkul and C. M. Bishop, Microstructural modeling and design of rechargeable lithium-ion batteries, *Journal of the Electrochemical Society*, 152 (2005) A255-A263.

[118] R. E. Garcia and Y. M. Chiang, Spatially resolved modeling of microstructurally complex battery architectures, *Journal of the Electrochemical Society*, 154 (2007) A856-A864.

[119] M. Doyle, T. F. Fuller and J. Newman, Modeling of galvanostatic charge and discharge of the lithium polymer insertion cell, *Journal of the Electrochemical Society*, 140 (1993) 1526-1533.

[120] T. F. Fuller, M. Doyle and J. Newman, Simulation and optimization of the dual lithium ion insertion cell, *Journal of the Electrochemical Society*, 141 (1994) 1-10.

[121] M. B. Pinson and M. Z. Bazant, Theory of SEI formation in rechargeable batteries: Capacity fade, accelerated aging and lifetime prediction, *Journal of the Electrochemical Society*, 160 (2012) A243-A250.

Yifan Gao received his B.S. in physics from Peking University, China in 2005. He received his M.S. degree in physics from Georgia Institute of Technology, Atlanta, Georgia, USA in 2008. He is currently a Ph.D. candidate in Mechanical Engineering at Georgia Institute of Technology. His research interests are multiphysics analysis of nano-materials for energy applications, especially materials for next-generation Li-ion batteries.

Maenghyo Cho received his B.S. and M.S. degrees in aeronautical engineering from Seoul National University, Seoul, Korea and his Ph.D. degree in aeronautics and astronautics from University of Washington, Seattle, USA. In 1999, he joined the faculty of Seoul National University where he is currently a professor in the School of Mechanical and Aerospace Engineering. His research interests are in the fields of multi-scale mechanics, molecular dynamics, solid/structural mechanics, and computational mechanics.

Min Zhou received his PhD in Applied Mechanics from Brown University in 1993. He is a Professor of Mechanical Engineering and Materials Science and Engineering at Georgia Institute of Technology in Atlanta, Georgia, USA. He is also a WCU professor at Seoul National University in Korea. His research focuses on the multiphysics behavior of materials at several length and time scales, emphasizing computational modeling with atomistic and continuum simulations and experiments with laser interferometry and digital diagnostics.